CHARACTERIZATION OF DISORDERED CONDUCTIVE CARBON FILMS PREPARED BY THERMAL CVD FROM ACETYLENE PRECURSOR

MR. SOMBOON FONGCHAIYA

A THESIS SUBMITTED IN PARTIAL FULFILLMENT
OF THE REQUIREMENTS FOR
THE DEGREE OF MASTER OF SCIENCE (PHYSICS)
FACULTY OF SCIENCE
KING MONGKUT'S UNIVERSITY OF TECHNOLOGY THONBURI
2014

Characterization of Disordered Conductive Carbon Films
Prepared by Thermal CVD from Acetylene Precursor

Mr. Somboon Fongchaiya B.Sc. (Physics)

A Thesis Submited in Partial Fulfillment of the Requirement for
the Degree of Master of Science (Physics)
Faculty of Science
King Mongkut's University of Technology Thonburi
2014

Thesis Committee

…… Chairman of Thesis Committee
(Lect. Chumphon Luangchaisri, Ph.D.)

……. Member and Thesis Advisor
(Lect. Tula Jutarosaga, Ph.D.)

……. Member
(Asst. Prof. Natthapong Phinichka, Ph.D.)

……. Member
(Lect. Watchara Liewrian, Ph.D.)

หัวข้อวิทยานิพนธ์	การวิเคราะห์ข้อบกพร่องของฟิล์มคาร์บอนนำไฟฟ้าซึ่งเตรียมด้วยวิธีซีวีดีแบบขดลวดความร้อนจากแก๊สอะเซทิลีน
หน่วยกิต	12
ผู้เขียน	นายสมบูรณ์ ฟองชัยญา
อาจารย์ที่ปรึกษา	ดร.ตุลา จูฑะรสก
หลักสูตร	วิทยาศาสตรมหาบัณฑิต
สาขาวิชา	ฟิสิกส์
ภาควิชา	ฟิสิกส์
คณะ	คณะวิทยาศาสตร์
ปีการศึกษา	2557

บทคัดย่อ

การทดลองนี้ได้ทำการสังเคราะห์ฟิล์มคาร์บอนนำไฟฟ้าโดยวิธีซีวีดีแบบขดลวดความร้อนจากแก๊สอะเซทิลีน และได้ศึกษาลักษณะโครงสร้างผลึก ค่าสภาพต้านทานไฟฟ้าแบบแผ่น และค่าการส่องผ่านแสง ซึ่งการทดลองได้แบ่งออกเป็นสองตอน การทดลองตอนแรกเป็นการสังเคราะห์ฟิล์มคาร์บอนบนแผ่นเวเฟอร์ที่มีพื้นผิวเป็นซิลิคอนไดออกไซด์ รามานสเปกตรัมแสดงลักษณะโครงสร้างที่เป็นแกรไฟต์ มีค่าอัตราส่วน I_D/I_G ~0.7-0.9 มีขนาดของผลึก ~19-24 nm และค่าสภาพต้านทานไฟฟ้าแบบแผ่น 85-221 โอห์ม/ตารางเซนติเมตร เมื่ออุณหภูมิในการสังเคราะห์ที่เพิ่มขึ้นพบว่าค่าอัตราส่วน I_D/I_G และค่าความกว้างพีคของแกรไฟต์ (G peak) มีค่าเพิ่มขึ้น เนื่องจากความบกพร่องในโครงสร้างแกรไฟต์ที่เพิ่มขึ้น ส่งผลทำให้ขนาดของผลึกมีค่าลดลง ตอนที่สองเป็นการสังเคราะห์ฟิล์มคาร์บอนบนควอตซ์ รามานสเปกตรัมแสดงลักษณะโครงสร้างของคาร์บอนอสัณฐานที่มีการจัดเรียงตัวแบบ sp ผสมอยู่ มีขนาดของผลึก ~18 Å และค่าสภาพต้านทานไฟฟ้าแบบแผ่น ~0.6-9.1 กิโลโอห์ม/ตารางเซนติเมตร เท่ากันกับฟิล์มบางแกรไฟต์ อันเนื่องมาจากคุณสมบัติทางด้านไฟฟ้าของคาร์บอนที่มีการจัดเรียงตัวแบบ sp ผสมอยู่ในโครงสร้างของฟิล์ม ช่วยให้ฟิล์มคาร์บอนอสัณฐานมีการนำไฟฟ้าที่ดีขึ้น เมื่ออุณหภูมิที่ใช้ในการสังเคราะห์ที่เพิ่มขึ้น พบว่าความกว้างพีคของแกรไฟต์มีค่าลดลง และความกว้างพีคของคาร์บอนที่มีการจัดเรียงตัวแบบ sp มีค่าเพิ่มขึ้น เนื่องจากโครงสร้างของฟิล์มมีการจัดเรียงตัวของคาร์บอนในแบบ sp^2 ที่มากขึ้น และมีการจัดเรียงตัวของคาร์บอนในแบบ sp ที่ลดลง

คำสำคัญ : แกรไฟต์ฟิล์ม / แก๊สอะเซทิลีน / คาร์บอนอสัณฐาน / ซีวีดีแบบขดลวดความร้อน / สเปกตรัมรามาน

Thesis Title	Characterization of Disordered Conductive Carbon Films Prepared by Thermal CVD from Acetylene Precursor
Thesis Credits	12
Candidate	Mr. Somboon Fongchaiya
Thesis Advisor	Dr. Tula Jutarosaga
Program	Master of Science
Field of Study	Physics
Department	Physics
Faculty	Science
Academic Year	2014

Abstract

In this work, the conductive carbon films were prepared by thermal chemical vapor deposition (TCVD) from acetylene (C_2H_2) precursor. The electronic structure, sheet resistance and transparency were studied. This work contains two different experiments. In the first experiment, the carbon films were synthesized on texture SiO_2/Si wafers. The Raman spectra showed graphitic structure with a I_D/I_G ratio of 0.7-0.9. The estimated in-plane crystallite size (L_a) was found to be in the range of 19-24 nm. Sheet resistance of graphite films were in the range of 85-221 Ω/sq. The I_D/I_G ratio and the full width at half maximum (FWHM) of G peak increased with increasing the growth temperature. This is due to the increasing temperature result in increasing the number of disordered carbons in the films which caused the reduction of crystallite size. In the second experiment, carbon films were synthesized on quartz slides. The Raman spectra showed amorphous structure coexisted with sp carbon hybridization. The average crystallite size of ~18 Å was obtained from amorphous carbon films. The sheet resistances of the films was in the range of 0.6-9.1 kΩ/sq which the same as that of thin graphite films. The mixture of sp carbon hybridization in the films caused the reduction of sheet resistance. The FWHM of G band decreased while that of C band increased with increasing growth temperature because of the increase of carbon in sp^2 hybridization and decrease of sp hybridization fraction in the films.

Keywords : Acetylene / Amorphous Carbon / Graphite / Raman Spectrum / Thermal Chemical Vapor Deposition

ACKNOWNLEDGEMENTS

I would like to thank my advisor, Dr. Tula Jutarosaga, for all help and suggestions to finish this work. I am also thankful to the department of Physics, faculty of Science, King Mongkut's University of Technology Thonburi for all kinds of supports in terms of laboratory instruments and chemicals in this work. This work was partially supported by the Research Center in Thin Film Physics, Thailand Center of Excellence in Physics (ThEP Center) and Nation Research Council of Thailand. Finally, I'm gratefully to my mother and my sister to give me the trust and love.

CONTENTS

PAGE

LIST OF TABLES

TABLE **PAGE**

LIST OF FIGURES

FIGURE **PAGE**

LIST OF FIGURES (cont'd)

FIGURE **PAGE**

LIST OF ABBREVIATIONS AND SYMBOLS

a-C	=	Amorphous carbon
a-C:H	=	Hydrogenated amorphous carbon
a.u.	=	Arbitrary unit
BWF	=	Breit-Wigner Fano line shape
CVD	=	Chemical vapor deposition
D	=	Disorder peak
EDX	=	Energy dispersive x-ray spectroscopy
E_i	=	laser Raman excitation energy
E_q	=	Energy of phonon in Raman scattering
E_s	=	Scattered photon energy
E_{2g}	=	Raman Vibrational mode of graphite lie at ~1580 cm^{-1}
eV	=	Electron volt
FCVA	=	Filtered cathodic vacuum arc
FLG	=	Few layer graphene
G	=	Graphite peak
h	=	Plank ‘s constant
ħ	=	Plank’s constant h divided by 2π
k	=	Wave vector or Wave number
Ƙ	=	Dirac point
L_a	=	In-plane crystalline size
nc-G	=	Nano crystalline-graphite
PECVD	=	Plasma enhanced chemical vapor deposition
PLD	=	Pulsed laser ablation deposition
SEM	=	Scanning electron microscope
SWCNT	=	Single walled carbon nanotube
TCVD	=	Thermal chemical vapor deposition
ta-C	=	Tetrahedral amorphous carbon
ta-C:H	=	Hydrogenated tetrahedral amorphous carbon
ta-C:N	=	Nitrogen-doped tetrahedral amorphous carbon
T_{2g}	=	Raman vibrational mode of diamond lie at 1332 cm^{-1}
υ_F	=	Fermi velocity in graphene
$\tilde{\nu}_o$	=	Wavenumber of incident radiation
$\tilde{\nu}_M$	=	Wavenumber after radiation

CHAPTER 1 INTRODUCION

1.1 Background

More than a decade ago, carbon films have attracted materials scientist due to their various in properties depending on carbon bonding hybridization. Electronic ground state configurations of carbon structure can be divided into sp^3, sp^2 and sp bonding hybridizations. Diamond has a sp^3 bonding hybridization and is an insulating material with almost isotropic properties. Graphite has a sp^2 bonding hybridization and is a conductive with an anisotropic property. Carbyne has an sp bonding hybridization and is a monoatomic polymer. Carbynes are electronically similar to the case of single-walled carbon nanotubes (SWCNTs).

Carbon can be classified to graphite, nano-crystalline graphite, amorphous carbon (a-C), hydrogenated amorphous carbon (a-C:H), tetrahedral amorphous carbon (ta-C) and tetrahedral hydrogenated amorphous carbon (ta-C:H) depending on the disordered and the sp^3 fraction containing. Raman spectroscopy is a simple technique used to characterize various forms of carbon due to its features such as nondestructive nature, fast response with high resolution providing structural properties and electronic formation. Ferrari and Robertson described three-stage model to characterize and classify graphite, disordered carbon, amorphous carbon and tetrahedral amorphous carbon [1]. This model shows factors that control the position, intensity and width of G and D peaks. In this report, graphite films and a-C films were classified and characterized according to this model.

Chemical vapor deposition (CVD) is a common method to synthesis conductive carbon films. Using this method, carbon atoms segregated on top of the metal catalyst films (such as Fe, Cu, Ni, etc.) to form a few layer graphene (FLG) or graphite films (GF) [2-5]. Then, carbon films were separated and transferred to arbitrary substrate.
To avoid the transfer process, previously researchers have investigated the direct growth of graphite thin films on a-plane sapphire substrates without any catalyst metal films by CVD from ethanol gas [6, 7]. So in this report, we constructed Thermal Chemical Vapor Deposition (TCVD) system to synthesis carbon film on texture SiO_2/Si wafers and quartz slides without metal seed layer from acetylene precursor. For studied electronic structure, sheet resistance and transparency of carbon films.

The experiment was divided into 2 stages. First experiment, carbon films were grown on texture SiO_2/Si substrates. Raman spectra showed graphite structure with in-plane crystalline size (L_a) of 19-24 nm and had sheet resistance of ~84-221 Ω/sq. Second experiment, carbon films were grown on quartz substrates to investigated transparency and sheet resistance. The Raman spectra showed amorphous carbon structure coexisted with sp carbon hybridization. The sheet resistance of our amorphous sp-sp^2 carbon films has higher than theoretical and experiment of graphene but equivalent to thin graphite films because the sp carbon containing in the films.

1.2 Literature Review

Table 1.1 List of literature review in synthesis of FLG and GF from TCVD

Authors (Years)	Catalyst films	Summary
A. Reina and et al. (2009) [2]	Ni	Synthesized large area FLG films with 1 to 12 graphene layers on Ni and transferred to the large arbitrary substrates. These films could be materials candidate for electronic and optoelectronic applications.
X. Li and et al. (2009) [3]	Cu	Synthesized large area single layer graphene films with a small percentage (less than 5%) of the area having few-layer graphene (2-3 layers).
K.S. Kim and et al. (2009) [4]	Ni	Synthesized large area graphene films, and presented two different methods for transfer graphene on Ni films to arbitrary substrates. The transferred graphene films showed very low sheet resistance of 280 Ω/sq with 80% transmittance.
W.W. Cai and et al. (2009) [5]	Cu and Ni	Synthesized large area few layer graphene and graphite films. These films were transferred to glass slides after dissolving few-layer graphene or graphite films on Ni films in an aqueous solution of $Fe(NO_3)_3$. The sheet resistance of these films of 200 Ω/sq with 85% transmittance.
Y. Miyasaka and et al. (2011) [6]	Without	They had examined the directly graphite thin films on nonpolar a-sapphire substrates without catalyst metals by alcohol-CVD. Graphite thin films consisted of nanograins of multilayer graphene on a-sapphire substrates.

1.3 Objective

- Understanding and optimize Thermal Chemical Vapor Deposition (TCVD) systems.
- To synthesize carbon films on substrate texture SiO_2/Si wafer and quartz without catalyst metal films by TCVD from acetylene precursor.
- To characterize various form of carbon films by Raman spectroscopy.
- To investigate sheet resistance and transparency of carbon films.

1.4 Scope of this work

- Construct simple TCVD systems to synthesis carbon films.
- Deposit carbon films by TCVD from acetylene precursor on texture SiO_2/Si and on quartz slides.
- Characterize carbon films by Raman spectroscopy, X-ray diffractometer (XRD), scanning electron microscope (SEM), mapping mode energy-dispersive X-rays (EDX), 4-point probe measurement and UV-Vis spectroscopy.

CHAPTER 2 THEORETICAL BACKGROUND

2.1 Carbon materials

Figure 2.1 shows the crystal structure of hexagonal single crystal graphite and diamond structure [8]. In the graphite phase of Figure 2.1 (left), the structure is highly anisotropic, exhibiting semi-metallic behavior in the basal (ab) plane and poor electrical conductivity in c-axis. In the diamond phase, the structure is an isotropic, cubic wide gap insulator (5.5 eV). The physical properties in the nature of graphite and diamond, graphite has stiffest materials (has the highest in-plane elastic modulus), opaque (black transparency), and very well in conductor while diamond is the hardest materials, highly transparent and low in conductivity. The comparison of properties of graphite and diamond [9] was reported on the table 2.1.

Bulk graphite is the stable phase under normal conditions, as indicated by the P-T phase diagram [10] of Figure 2.2. Under the ambient of high pressure and high temperature, carbon was transform to diamond structure. On the other hand, when the pressure and temperature was reduced, diamond structure transformed back to the graphite phase.
Carbon has an atomic number of 6 and is in a $1s^2\ 2s^2\ 2p^2$ electronic ground state configuration. In the graphite structure, strong in-plane bonds are formed between a carbon atom and three nearest-neighbors form 2s, $2p_x$, and $2p_y$ orbitals; this bonding arrangement is denoted by sp^2 (see Figure 2.3). The remaining electron with a p_z orbital provides only weak interplanar bonding, but is responsible for the semimetallic electronic behavior in graphite. In contrast, the carbon atoms in the diamond structure are tetrahedrally bonded to their four nearest-neighbors using linear combination of 2s, $2p_x$, $2p_y$ and $2p_z$ orbitals in a sp^3 configuration (see Figure 2.3) [11]. The different in the structure arrangement of these allotropic forms of carbon bring about the wide differences in their physical properties.

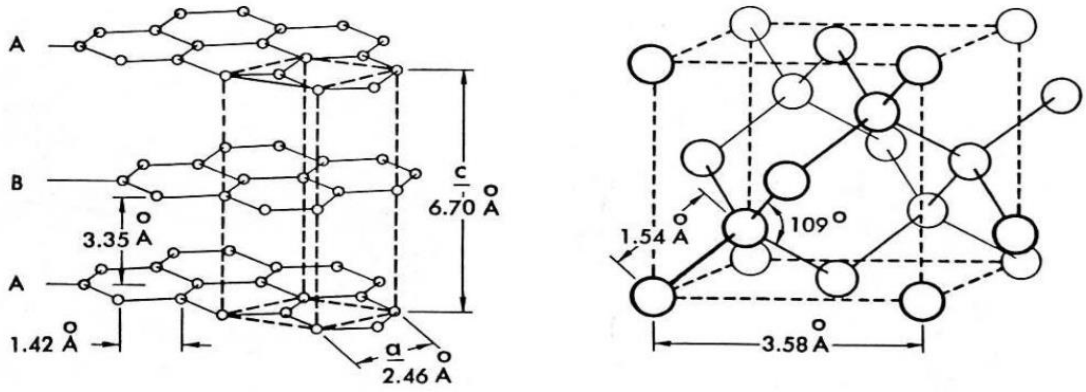

Figure 2.1 (left) Hexagonal single crystal graphite and (right) diamond structure [8].

Table 2.1 Properties of graphite and diamond [9]

Properties	Graphite		Diamond
	a-axis	c-axis	
Lattice structure	Hexagonal		Cubic
Space group	$P6_3/mmc$ (D_{6h}^4)		$Fd3m$ (O_h^7)
Lattice constant at 300 K (Å)	2.46	6.70	3.57
Atomic density (C atoms/cm^3)	1.14 x 10^{23}		1.77 x 10^{23}
Specific gravity (g/cm^3)	2.26		3.515
Specific heat (cal/g·K)	0.17		0.12
Thermal conductivity at 300 K (W·cm·K)	30	0.06	~25
Binding energy (eV/C atom)	7.4		7.2
Debye Temperature (K)	2500	950	1860
Bulk modulus (GPa)	286		42.2
Elastic moduli (GPa)	1060	36.5	107.6
Compressibility (cm^2/dyn)	2.98 x 10^{-12}		2.26 x 10^{-13}
Mohs hardness	0.5	9	10
Band gap (eV)	-0.04		5.47
Carrier density (10^8/cm^3 at 4 K)	5		0
Electron mobility at 300 K (cm^2/Vsec)	20,000	100	1800
Hole mobility at 300 K (cm^2/Vsec)	15,000	90	1500
Resistivity (Ω·cm)	50 x 10^{-6}	1	~10^{20}
Dielectric constant at 300 K (low ω)	3	5	5.58
Breakdown filed (V/cm)	0	0	10^7
Magnetic susceptibility (10^{-6} cm^3/g)	-0.5	-21	-
Refractive index (visible)	-	-	2.4
Melting point (K)	4450		4500
Thermal expansion at 300 K (/K)	-1 x 10^{-6}	+29 x 10^{-6}	~1 x 10^{-6}
Velocity of sound (cm/sec)	~2.63 x 10^5	~1 x 10^5	~1.96 x 10^5
Highest Raman mode (cm^{-1})	1582	-	1332

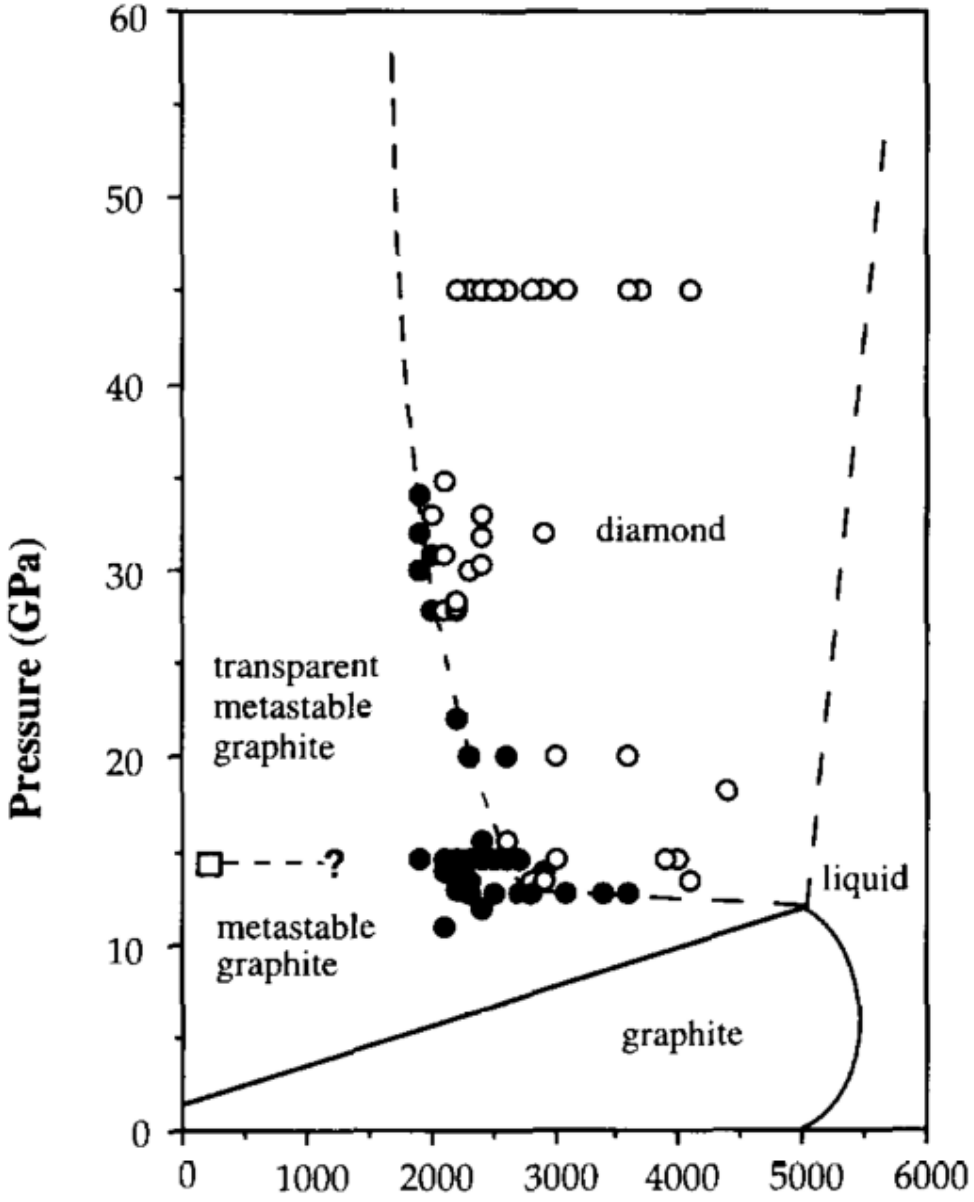

Figure 2.2 Pressure and temperature (P-T) phase diagram of carbon materials [10].

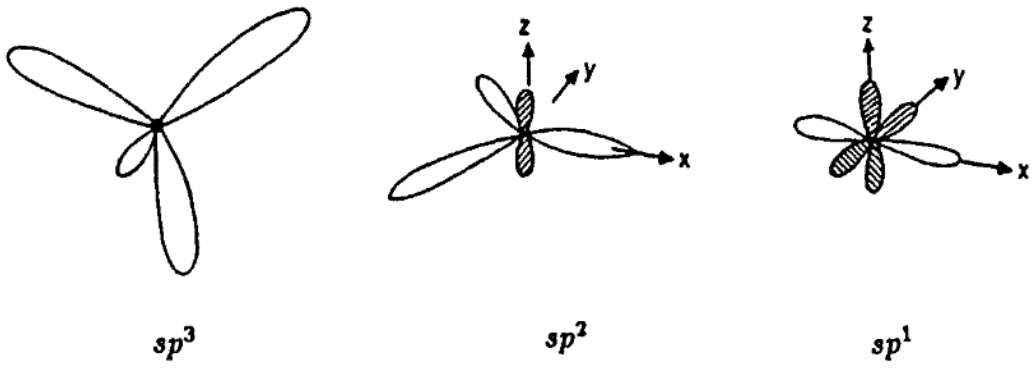

Figure 2.3 sp^3, sp^2 and sp hybridized bonding [11].

2.2 Graphene

Graphene is a two-dimensional sheet of hexagonal sp^2 carbon plane. It was attracted from scientists due to the extraordinary properties in electrical and thermal properties. Each carbon atom in hexagonal planes shared σ bond. The forth bond oriented in z direction is a π bond. The π orbitals on each carbons can visualized to a pair of symmetric lobes oriented along the z-axis and centered on the nucleus (see sp^2 C on Figure 2.3). A pair of symmetric lobes referred to as the π band (lower energy valence band) and π* bands (higher energy conduction band). These bands are corresponding with peculiar electronic properties of graphene.

The structure of the electronic energy bands and Brillouin zones for graphene was first calculated using tight-binding approximation in 1947 by Wallace [12]. The π and π* bands gaps close at the corners of the Brillouin zone or the Ҡ-point (called Dirac points). As a result, the π-band dispersion is approximately linear around the Ҡ-point:

$$E = \hbar v_F |k| \tag{2.1}$$

where k is the wave vector measured from Ҡ, ħ is Planck' s constant h divided by 2π, and v_F is the Fermi velocity in graphene, approximately 106 m/s.

A linear dispersion normally characterizes particles whose kinetic energy vastly exceeds their rest mass energy. Electron in graphene thus behave like photon or other ultra-relativistic particles (such as neutrinos), with an energy-independent velocity v_F that is approximately 300 times smaller than the speed of light.

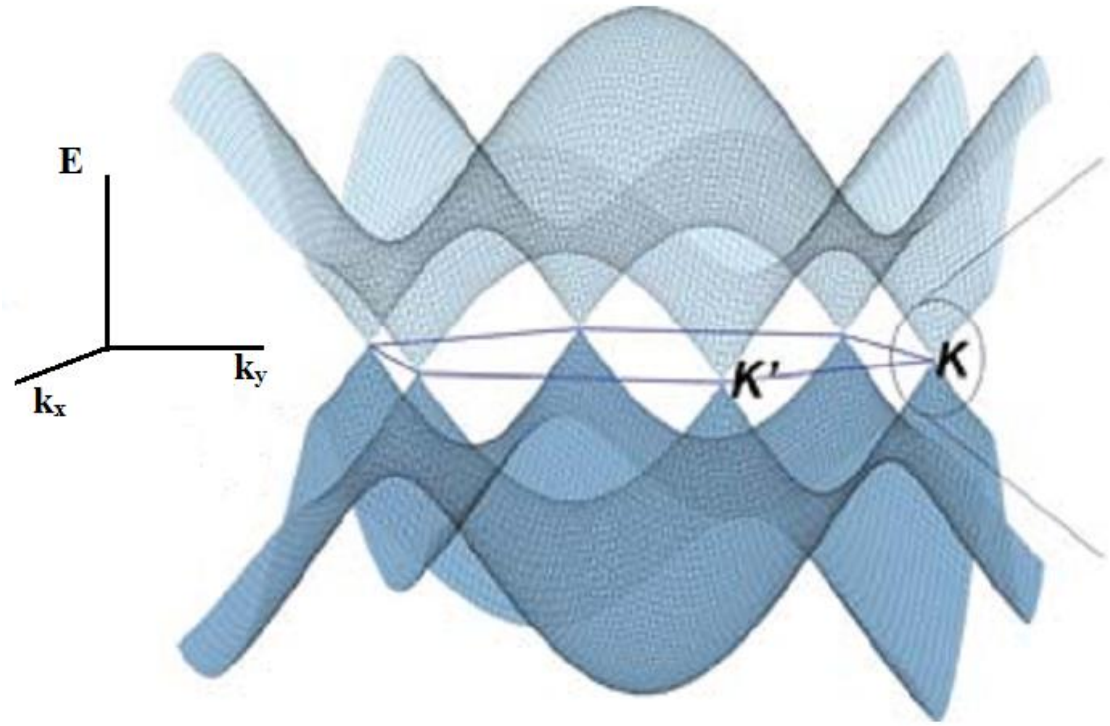

Figure 2.4 Tight-binding band structures of graphene [13].

2.3 Diamond-like carbon

Diamond-like carbon (DLC) is an amorphous carbon (a-C) or hydrogenated amorphous carbon (a-C:H) films with a high fraction of metastable sp^3 carbon bonding. It has extreme properties similar to diamond but cheaper to produce. The DLC films have widely used in protective coatings such as optical windows, magnetic storage disks, car parts and as micro-electromechanical devices (MEMs).

The typical of DLC can be displayed on a ternary phase diagram. Figure 2.5, shows the fraction of sp^3 C, sp^2 C and H bonding. This diagram was first derived by Jacob and Moller [14]. The digram consists of three main regions.

First region is sp^2 C and sp^3 C fraction without H contents. There are many types of a-Cs with disordered graphitic such as soot, chars, glassy carbon, and evaporated a-C at the lower left hand corner. The a-Cs with higher sp^3 content produced by sputtering is DLC. At the higher sp^3 content, a-C is a tetrahedral amorphous carbon (ta-C). The ta-C was prepared by filtered cathodic vacuum Arc (FCVA) and pulse laser ablation deposition (PLD).

Second region is sp^3 C and H fraction. On the bottom right, when the H content is highest, the films could not form. The boundary line of this region is defined by polyethylene $(CH_2)_n$ and polyacethylene $(C_2H_2)_n$.

Third region is sp^2 C and H fraction. Hydrogenated amorphous carbon (a-C:H) was produced by Plasma enhanced chemical vapor deposition (PECVD) of hydrogen molecules, reactive sputtering of graphite in atmosphere including H, or by ion beam deposition from a hydrocarbon gas precursors. The a-C with H content can be divided to a-C:H films with highest H content (40-60 at %) and a-C:H films with intermediate H content (20-40 at %).

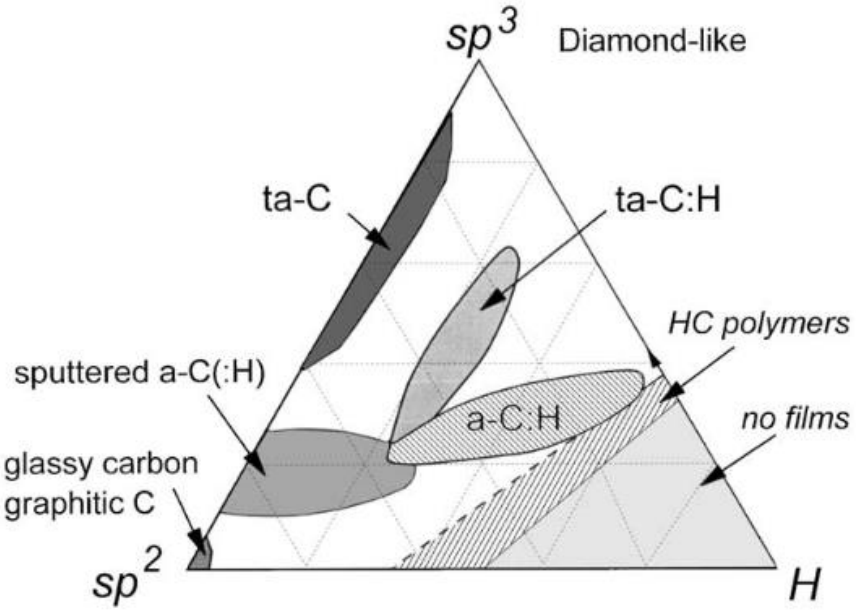

Figure 2.5 Ternary phase diagram of bonding in amorphous carbon-hydrogen alloy [14].

2.4 Raman scattering principle

When shinning monochromatic light on a material, the absorption of photon occurred on the material to cause shook of electron energy, the shook electron was excited from ground state to virtual energy state. The incident of energy state is $E_i = hc\tilde{v}_0$ and excited electron energy is $E_f = hc\tilde{v}_m$ where $\tilde{v}_o$ and $\tilde{v}_m$ is wavenumber of incident radiation and after radiation, respectively. The shook electron was scattered and transferred energy to neighbor electron, this process was changed Polarizabilty of an atom in a material. If scattered electrons have energy after scatter equal with incident scatter (elastic scattering) is called Rayleight scattering. Another process, if the scattered electron has lost or gain energy (inelastic scattering) is called Raman scattering (Figure 2.6).

In Raman scattering divided into two processes: Stoke Raman scattering and Anti-stoke Raman scattering [15,16].
Stoke Raman scattering is the process has lost energy $hc(\tilde{v}_o - \tilde{v}_M)$ in creating a phonon, scattered of photon will be shifted to lower wavenumber.
Anti-Stoke Raman scattering is the process has gain energy $hc(\tilde{v}_0 + \tilde{v}_M)$ in creating a phonon, scattered of phonon will be shifted to higher wavenumber.
Raman spectrum is a plot of the scattered intensity I_s as a function of $E_i - E_s$ (Raman shift, Figure 2.7). The conservation energy of Raman process:

$$E_s = E_i \pm E_q, \tag{2.2}$$

where E_s is scattered photon energy, E_i is laser excitation energy and E_q is energy of phonon that is created ($+E_q$) or annihilated ($-E_q$) in the inelastic Raman scattering event. The energy of Stoke process occurs at positive energy while Anti-Stoke process occurs at a negative energy.

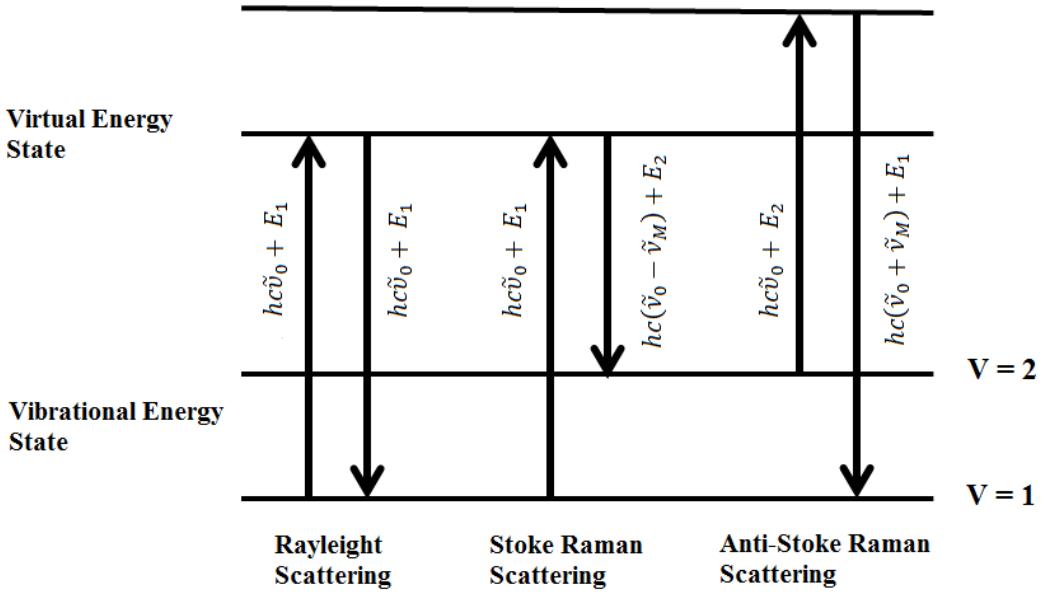

Figure 2.6 Energy-level diagram of an energy transfer model of Rayleight scattering, Stoke Raman scattering, and Anti-Stoke Raman scattering.

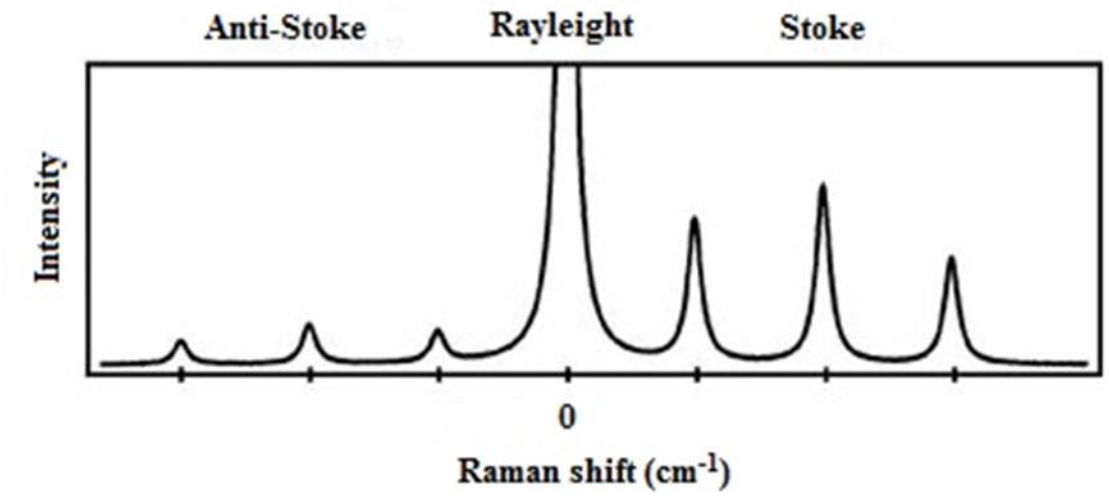

Figure 2.7 Raman spectrum of Rayleight Scattering, Stoke Raman scattering and Anti-Stoke Raman scattering [16].

2.5 Raman spectroscopy of disordered and amorphous carbon

Raman spectroscopy is a standard nondestructive tool for characterization of crystalline, nanocrystalline and amorphous carbons. The Raman spectra of disordered graphite shows G-peak and D-peak (see Figure 2.8). The G-band of graphite centered at 1581 cm^{-1} has E_{2g} symmetry. This refers to the in-plane bond stretching motion of pairs of sp^2 C atoms, Figure 2.9(A). This mode does not require the presence of sixfold ring, so it occurs at all sp^2 sites, not only those in rings. It always lies in the range of 1500-1630 cm^{-1}, as it does in aromatic and olefinic molecules. The D peak around 1355 cm^{-1} is a breathing mode of A_{1g} symmetry involving phonons near the K zone boundary, Figure 2.9(B). This mode disappeared in perfect graphite and only becomes active in the presence of disorder. The D mode is dispersive; it varies with photon excitation energy, even when the G peak is not dispersive.

In Figure 2.8, the Raman spectrum are considered to depend on

(1) Clustering of the sp^2 phase
(2) Bond disorder
(3) Presence of sp^2 rings or chains and
(4) The sp^2/sp^3 ratio

The shape of the Raman spectrum depends on these factors.

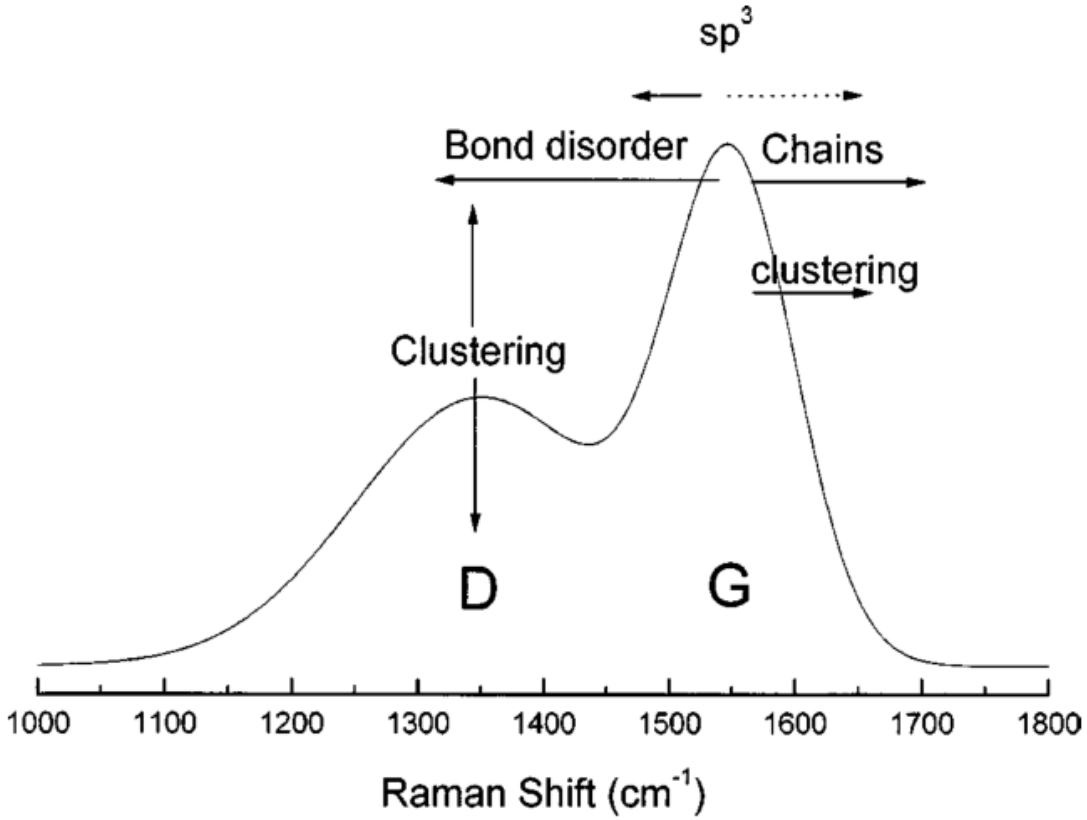

Figure 2.8 Schematic diagram of influence on the Raman spectra. A dotted arrow marks the indirect influence of the sp^3 content on increasing G position [1].

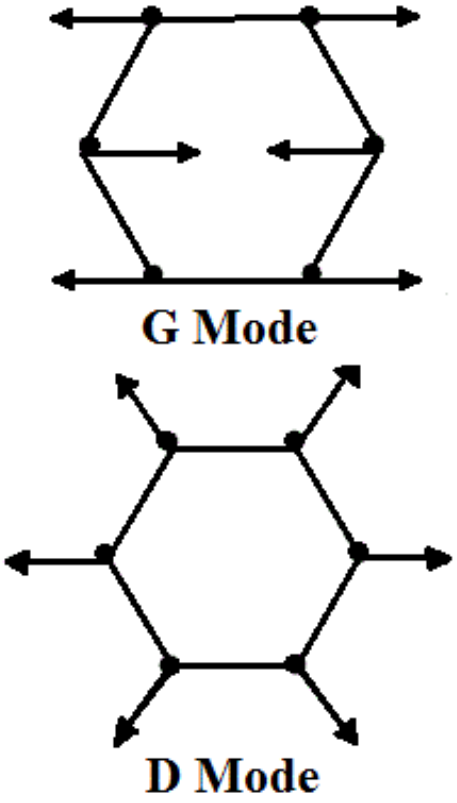

Figure 2.9 Carbon motions in the (a) G and (b) D modes [1].

Three stage model

Ferrari and Robertson described the behavior of Raman spectra in all of microcrystalline and amorphous carbon can classify using a three-stage model. The amorphization trajectory ranging from graphite to ta-C (or diamond) consists of three stages, which are (Figure 2.10)

(1) Graphite→nanocrystalline graphite (nc-G)
(2) Nanocrystalline graphite→a-C, and
(3) a-C→ta-C (~100% sp^3, defected diamond)

For simplicity, the evolution of G-peak position and I_D/I_G were considered. Except where differently stated, Figure 2.10 refer to Raman data at laser excitation wavelength 514 nm.

Stage 1: from graphite to nanocrystalline graphite

The main effects in the evolution of the Raman spectrum in this stage are the following.

- The G peak moves from 1581 to ~1600 cm^{-1} due to the reduction of the grain size (L_a) within an ordered graphite layer.
- The D peak appears and I_D/I_G increase following Tunistra & Koening (TK) relation, I_D/I_G α $1/L_a$ [Figure 2.11 right hand of boundary line].
- There is no dispersion of the G mode.

Stage 2: from nanocrystalline graphite to a-C

The main effects in the evolution of the Raman spectrum are

- The G peak decreases from 1600 to ~1510 cm^{-1} due to the increasing bond angle and bond-bending disorder and the presence of non sixfold rings softens.
- The TK equation is no longer valid: I_D/I_G α Number of aromatic rings in the cluster (M) α L_a^2.
- $I_D/I_G \rightarrow 0$.
- Increasing dispersion of the G peak occurs.

For more disorder, clusters decrease in number become smaller and more distorted, until they open up. As the G peak is just related to the relative motion of sp^2 C atoms, the I_D will now decrease respect to I_G and TK relationship is no longer hold, as shown in Figure 2.11.

The structure of a-C at the end of stage 2 consists of mainly sp^2 sites in puckered ring-like configurations (consisting of five-, six-, seven-, and eightfold distorted rings), and few if any sp^3 sites (maximum 20% sp^3).

Stage 3: From a-C to ta-C

The main effects in the evolution of the Raman spectrum are as follows.

- The G peak increase from ~1510 to ~1570 cm^{-1} due to the change of sp^2 configuration from rings to olefinic groups, with their higher vibrational frequencies lying above the band limit of graphite.
- I_D/I_G is very low or 0. (absence of D peak)
- Dispersion of the G peak occurs.

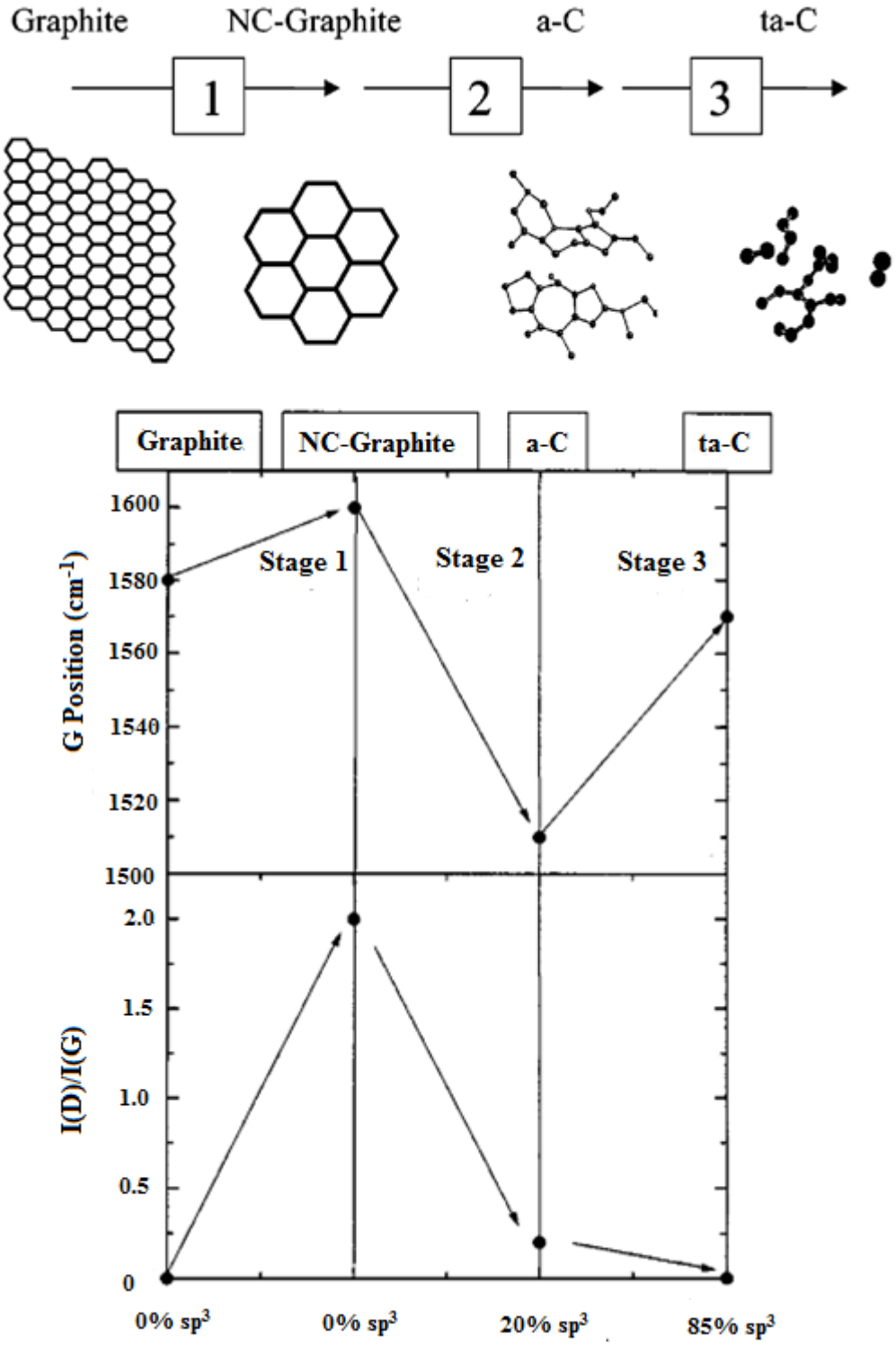

Figure 2.10 Three stage model of the variation of the Raman G position and the I_D/I_G with increasing disorder [1].

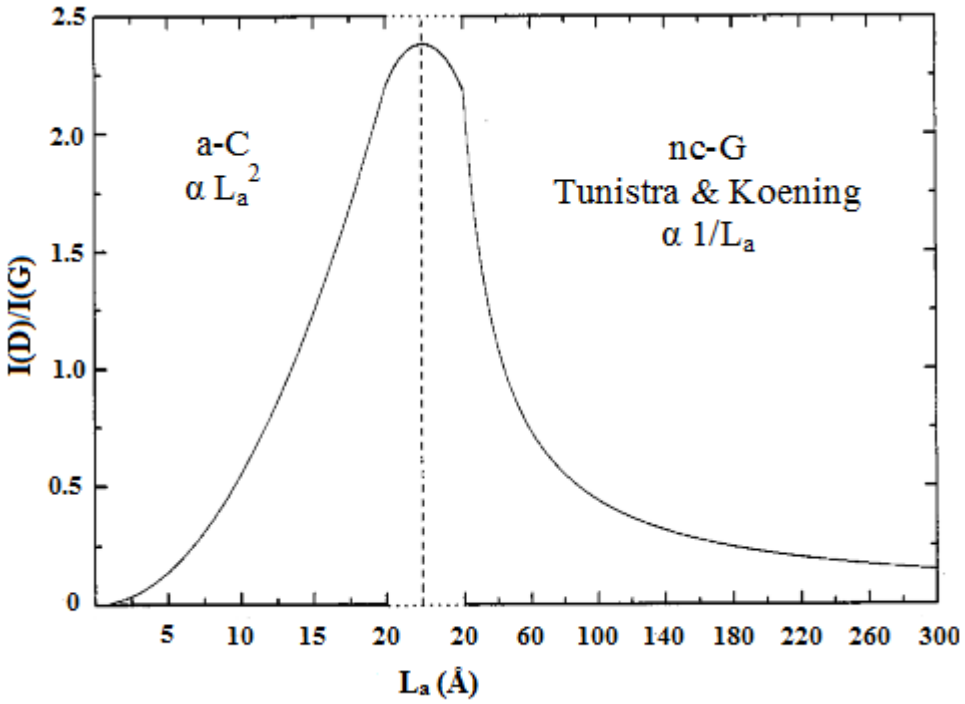

Figure 2.11 Variation of the I_D/I_G ratio with L_a. The broad transition between the two regimes indicated [1].

2.6 Measuring the crystalline size of nanographite by Raman spectroscopy

Cancado et al. presented a systematic study of the I_D/I_G in nanographite samples with different crystalline size (L_a) and using different excitation laser energies (See Figure 2.12). The crystalline size of the nanographite was obtained by X-ray diffraction (XRD) using synchrotron radiation and directly from scanning tunneling microscopy. The result shows that I_D/I_G is inversely proportional to the fourth power of the laser energy used in the experiment (see Figure 2.11). Thus, a general equation for determination of L_a using any laser energy in the visible range is given by

$$L_a(nm) = \frac{560}{E_{laser}^4}\left(\frac{I_D}{I_G}\right)^{-1} = (2.4 \times 10^{-10})\lambda_{laser}^4\left(\frac{I_D}{I_G}\right)^{-1} \quad (2.3)$$

where the laser excitation is given in term of both E_{laser} (eV) or wavelength (nm).

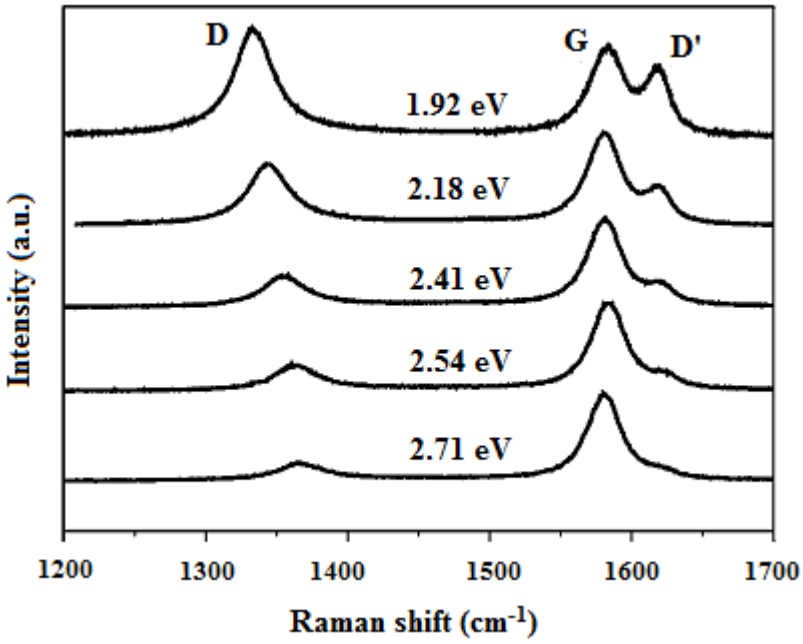

Figure 2.12 Raman spectra of the sample heat treated at 2000ºC, for five different laser energy values (1.92, 2.18, 2.41, and 2.71 eV) [17].

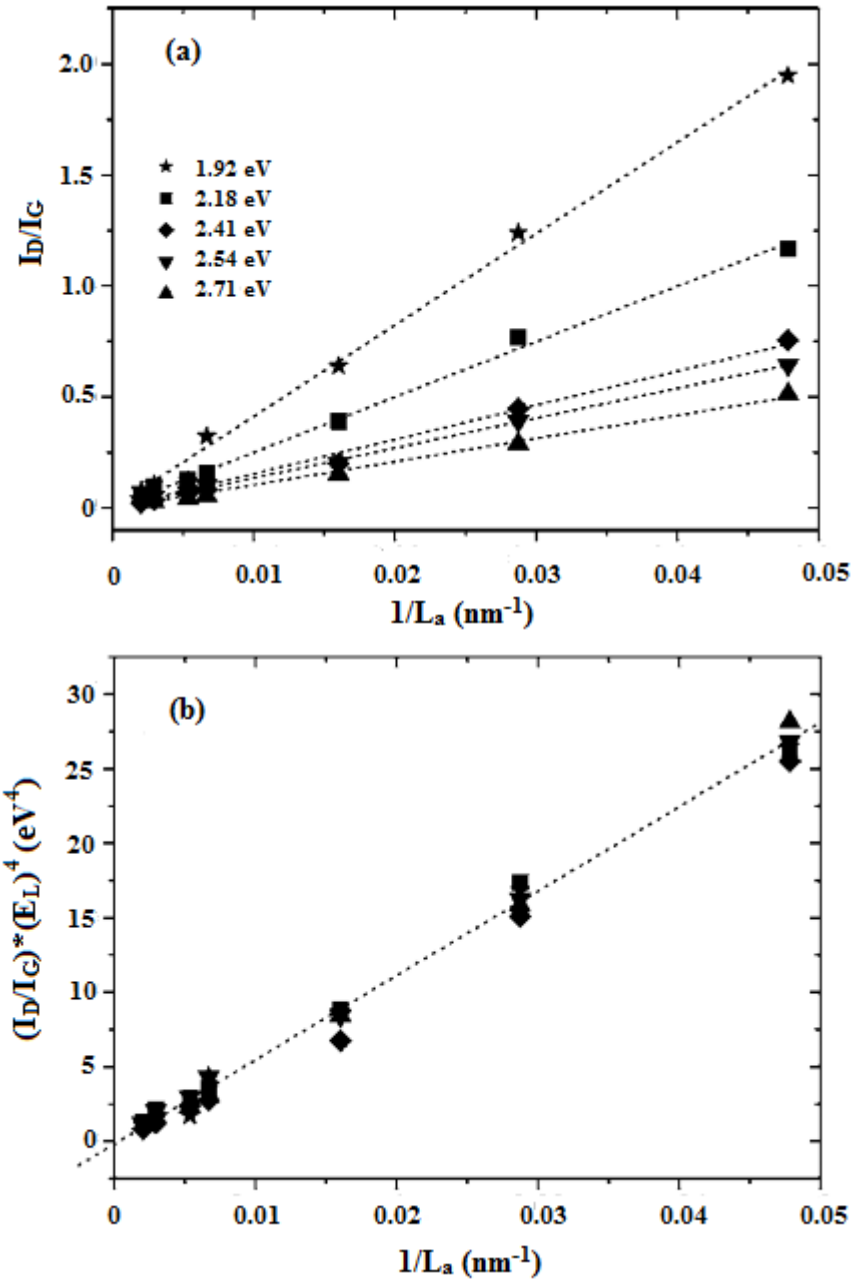

Figure 2.13 (a) Plot of the ratio of the integrated intensities of the D and G band (I_D/I_G) vs $1/L_a$ for all spectra obtained with the five different excitation laser energies (b) all of experimental results shown in part (a) collapse in the same straight line in the $\left(\frac{I_D}{I_G}\right) E_l^4$ vs $1/L_a$ plots [17].

2.7 Raman spectroscopy of graphene

The comparison of Raman spectra between bulk graphite and graphene at laser excitation wavelength 514 nm was shown in Figure 2.14. Both of Raman spectra shows strong G and 2D (maybe denoted by G') peak. These peaks are the Raman signature for sp^2 carbons at the peak position of ~1580 cm^{-1} and ~2500-2800 cm^{-1}, respectively. The 2D peak of bulk graphite consists of two components peaks, $2D_1$ and $2D_2$, while the graphene has a one component peak. The ratio of I_{2D}/I_G of graphene structure is about 2 to 4 and that of the bulk graphite is about 0.25 to 0.5. Single layer graphene, bi-layer graphene and many-layer graphene can be classified using the feature from 2D band. As the number of graphene layers increase, the 2D peak tend to broaden and shift to larger wavenumber (Figure 2.15) due to the increase of peak components. However, graphene that has more than five layers the Raman spectrum becomes hardly distinguishable from the bulk graphite. Thus, Raman spectroscopy could distinguishable graphene less than five layers.

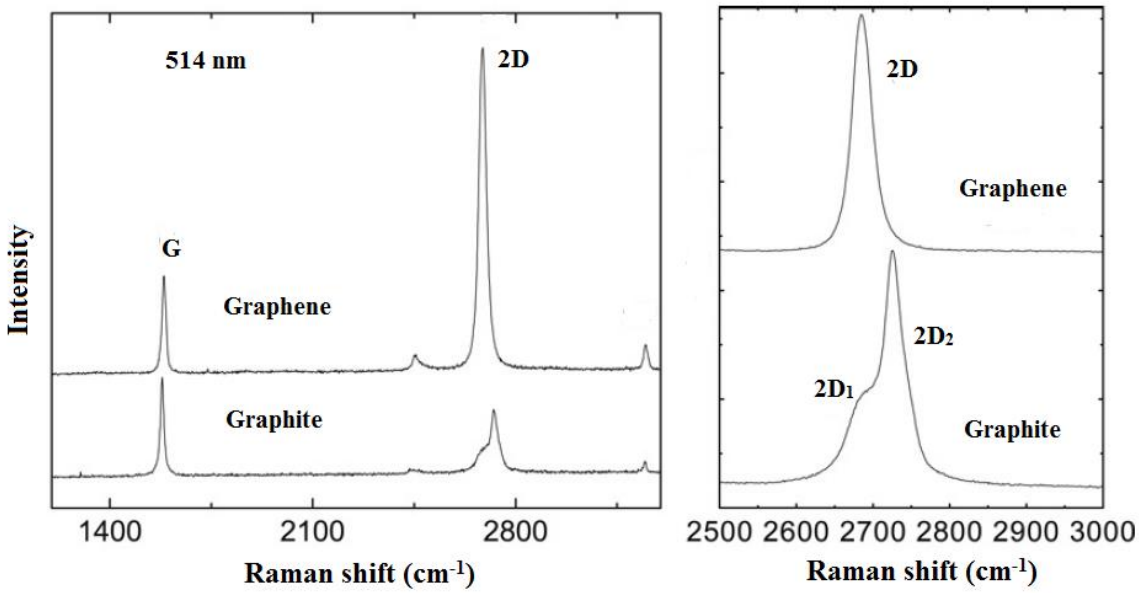

Figure 2.14 Comparison of Raman spectra at 514 nm for bulk graphite and graphene [18].

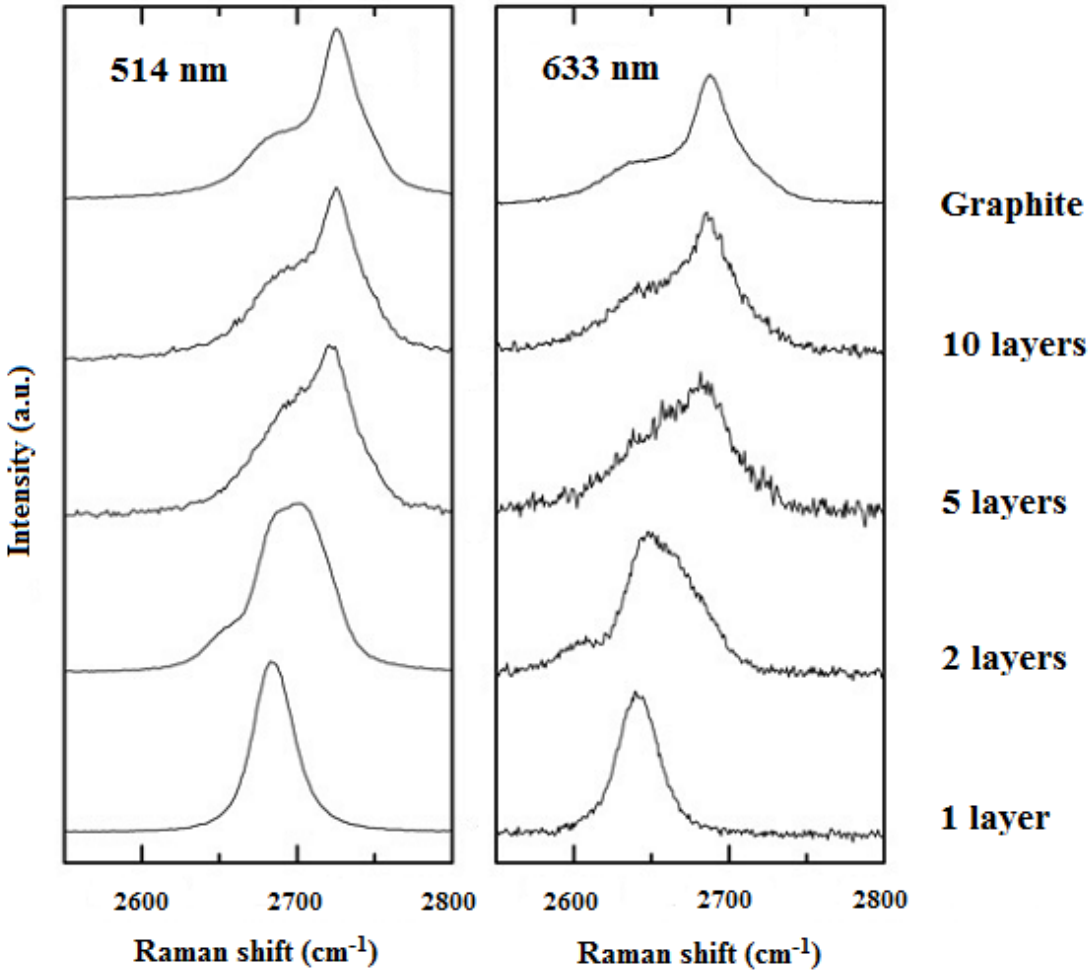

Figure 2.15 Evolution of the spectra at 514 and 633 nm with the number of graphene layers [18].

CHAPTER 3 EXPERIMENT

In this chapter, the procedure to synthesis carbon films on texture SiO_2/Si wafers and quartz slides using TCVD was described. In the first experiment, graphite films were synthesized on texture SiO_2/Si wafers to investigate the electronic structure and sheet resistance. For the second experiment, amorphous sp-sp^2 carbon was synthesized on quartz slides to investigate the electronic structure, transparency and sheet resistance.

3.1 Experiment apparatus and chemical

- Acetylene gas (C_2H_2) 99.6% purity as a carbon source.
- Argon-Hydrogen gas (concentration, Ar 90% and H_2 5%).
- Nitrogen gas (N_2) 99.999% purity.
- Substrate, texture SiO_2/Si wafers and Quartz slides.
- Ethanol (C_2H_6O) for cleaning substrate.
- Home-made TCVD system (Figure 3.1) consists of tube furnace, small rotary pump, pressure gauge, quartz tube (diameter 5 cm) and flow meter (correlated flow meter and mass flow controller.

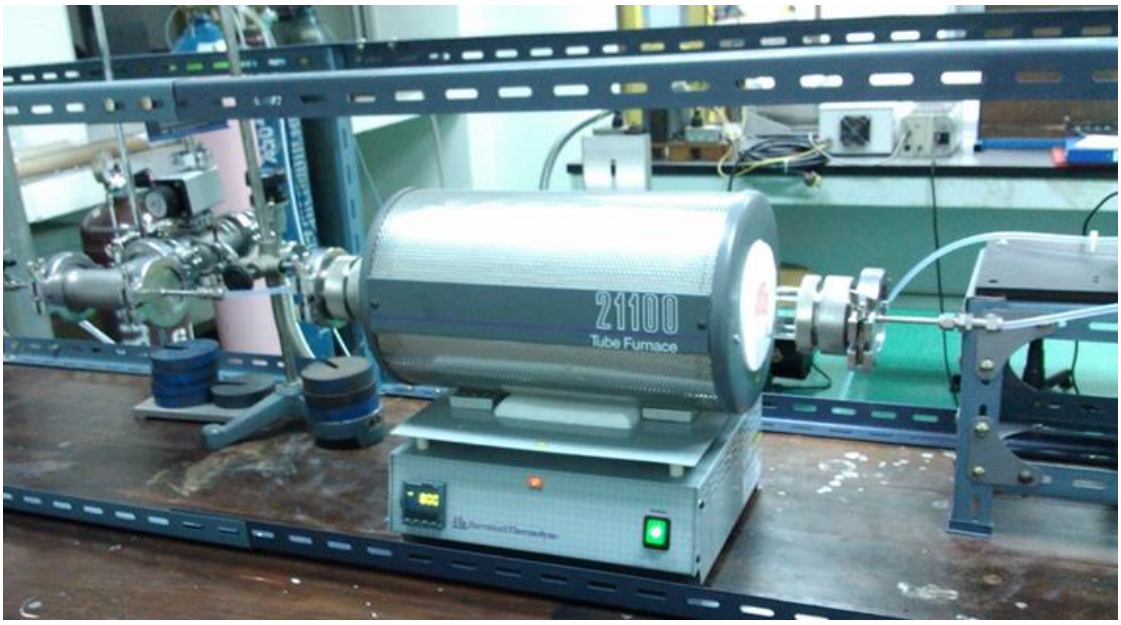

Figure 3.1 Hand-made setup of TCVD system in our lab.

3.2 Methods

Both of experiment used the same growth temperature 800 ºC and 900 ºC. The temperature profiles of tube furnace at 800 ºC and 900 ºC are display on the Figure 3.2(A) and Figure 3.2(B), respectively. The temperature at the center of tube furnace (apart from the both side 20 cm), with the set point 800 ºC and 900 °C, was measured using thermocouple (type K). The readout temperature were 792 ºC, and 900 ºC, respectively. The temperature at the center of tube furnace was equivalent to the set point. The profiles of the temperature at different position in the furnace for the set point of 800 ^{o}C and 900 ^{o}C are shown in Figure 3.10.

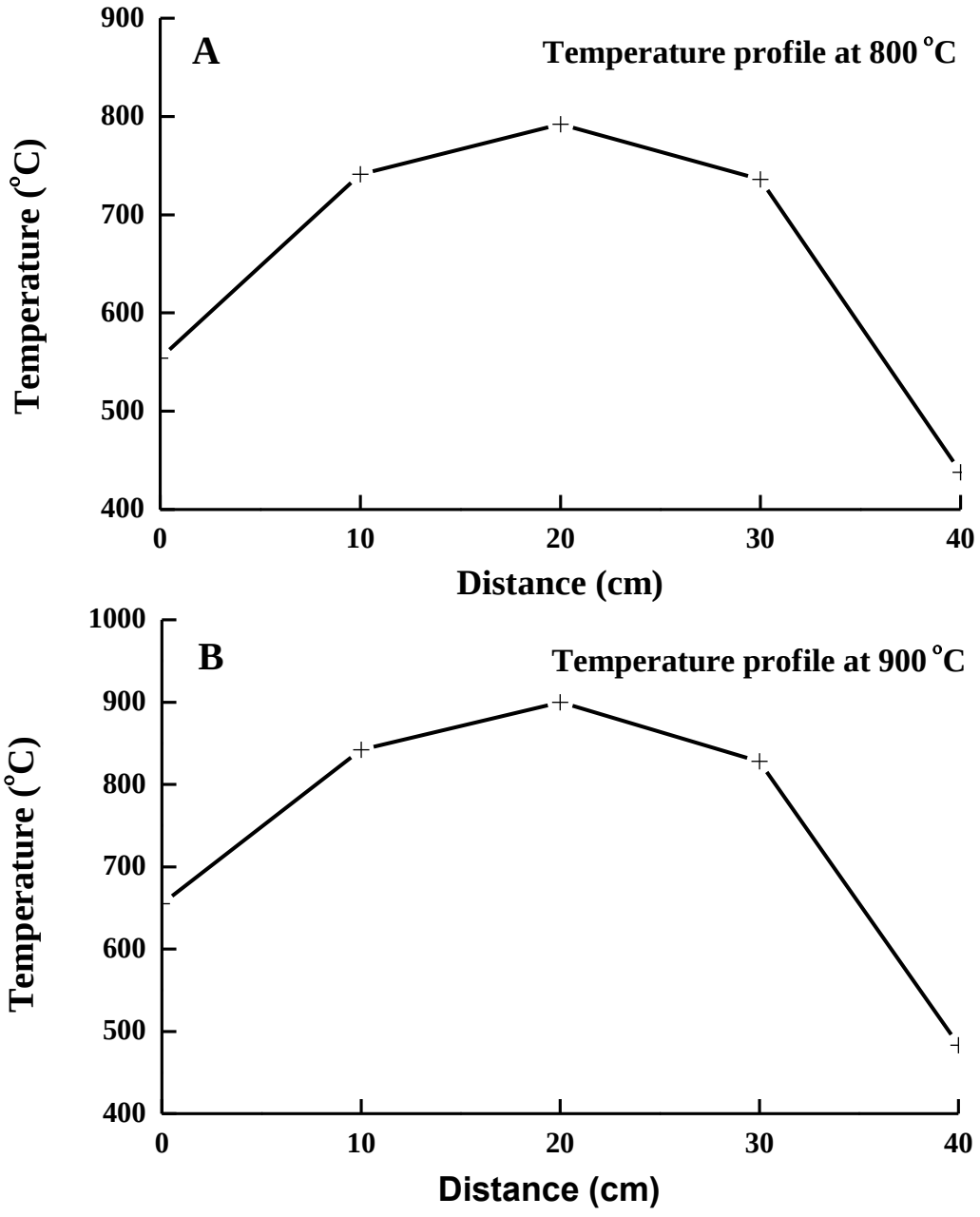

Figure 3.2 Temperature profiles in the tube furnace at (A) 800 ºC and (B) 900 °C.

3.2.1 Graphite films on texture SiO_2/Si wafer

Graphite films (GF) were coated on unpolished side of SiO_2/Si wafers by TCVD from acetylene precursor at 800 °C and 900 °C under atmospheric pressure. The schematic diagram of TCVD and profile of procedure for synthesis graphite was displayed on the Figure 3.3 and Figure 3.4, respectively.

The sequences of process flow are

- First stage, substrates were put in an alumina boat and placed at the center of quartz tube and then the furnace was heated up to the desired temperatures (800 °C and 900 °C) under the N_2 ambient with flow rate of 400 sccm at atmosphere pressure.
- Second stage, when the reactor reach the desired temperature, N_2 gas was turned off and Ar:H_2 gas with the flow rate of 150 sccm was introduced to the system for 30 minutes to pretreated substrate surfaces.
- Third stage, Ar:H_2 gas was then turned off and C_2H_2 gas was introduced to the system with C_2H_2 flow rate of 40 sccm for 40 minutes.
- Forth stage, the system was cooled downs to room temperature under N_2 gas ambient at atmospheric pressure.

Surface morphology and composition of the graphite films on the texture SiO_2/Si wafers were observed by Scanning Electron Microscope (SEM) and Energy-Dispersive X-ray Spectroscopy (EDX). Electronic structural and estimate in-plane crystalline sizes of graphite films was observed by Raman spectroscopy at excitation wavelength 514 nm. Sheet resistance of graphite films was measured by 4-point probe measurement. The result and discussion of GF was showed in chapter 4.1.

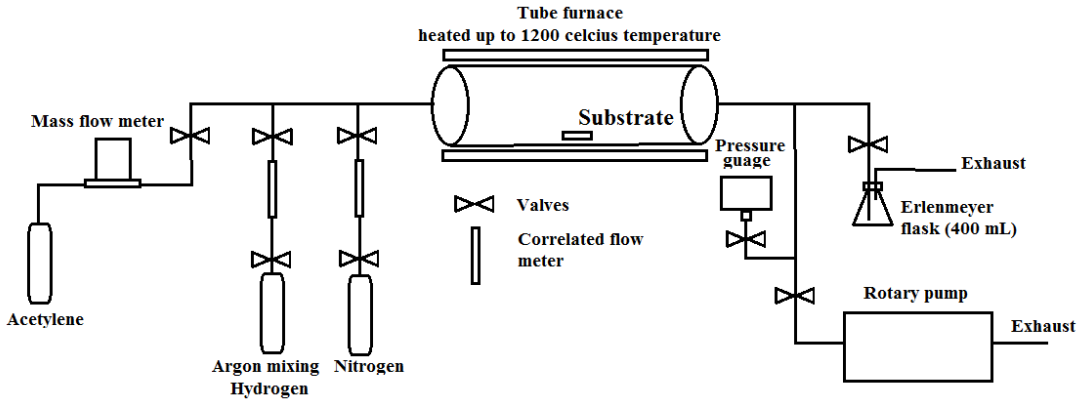

Figure 3.3 Schematic diagram of TCVD system used to grown graphite films.

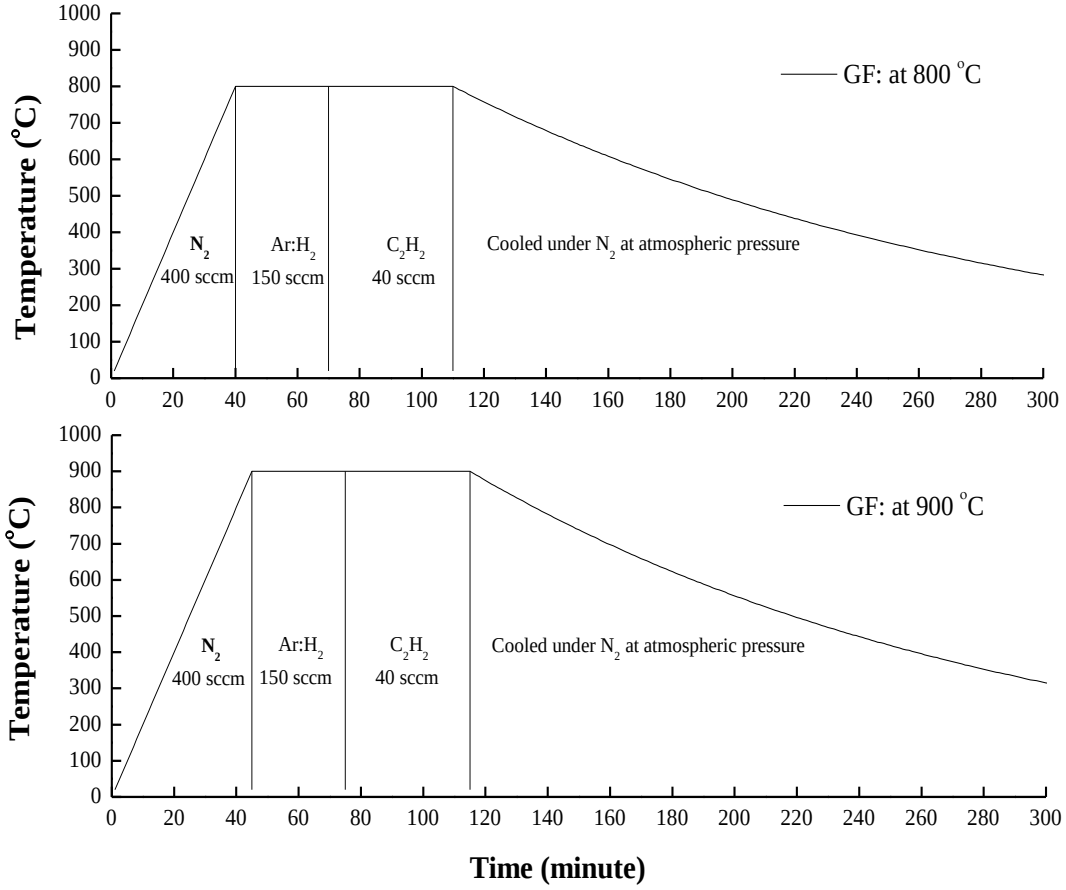

Figure 3.4 Flow of procedure to synthesis graphite films at (A) 800 °C and (B) 900 °C.

3.2.2 Amorphous sp-sp^2 carbon films on quartz slides

Amorphous sp-sp^2 carbon films deposited directly on quartz slides by TCVD from acetylene precursor at 800 °C and 900 °C under low vacuum (~15 mbar). The profile of procedure to synthesis amorphous sp-sp^2 carbon was displayed on the Figure 3.5.

The sequences of process flow are

- First stage, quartz slides (2 cm × 2 cm) were placed on the center of tube furnace. The system was vacuumed to 0.21 mbar by a rotary pump. Then, Ar-H_2 gas with flow rate of 200 sccm was introduced into the system. Then, the furnace was heated up to desirable temperature in the range of 800 to 900 °C under Ar-H2 gas.
- Second stage, when the temperature reached the set temperature, Ar-H_2 gas was turn off and C_2H_2 flow varied condition 100 sccm and 150 sccm into the system for 1 hour at the pressure of ~15 mbar.
- Third stage, the system was then cooled down to the room temperature under N_2 gas flow rate of 15 sccm with vacuumed by rotary pump.

This experiment generated 4 samples labeled as S-800-100, S-900-100, S-800-150 and S-900-150. The capital S stands for sample, the first number as read from left to right indicate the temperature in ºC and the last number represents the C_2H_2 flow rate in sccm.

The electronic structure was evaluated by Raman spectroscopy at excitation wavelength of 758 nm. The surface morphology observed by SEM. The atomic percentage of all elements on the films evaluated by mapping mode EDX spectroscopy at 100X. The transmittance values (%T) at 550 nm evaluated by Ultraviolet –Visible (UV-Vis) spectroscopy in the range of 450-800 nm. The sheet resistance measured by 4-point probe measurement technique. The results and discussion of amorphous sp-sp^2 carbon films was showed in section 4.2 in chapter 4.

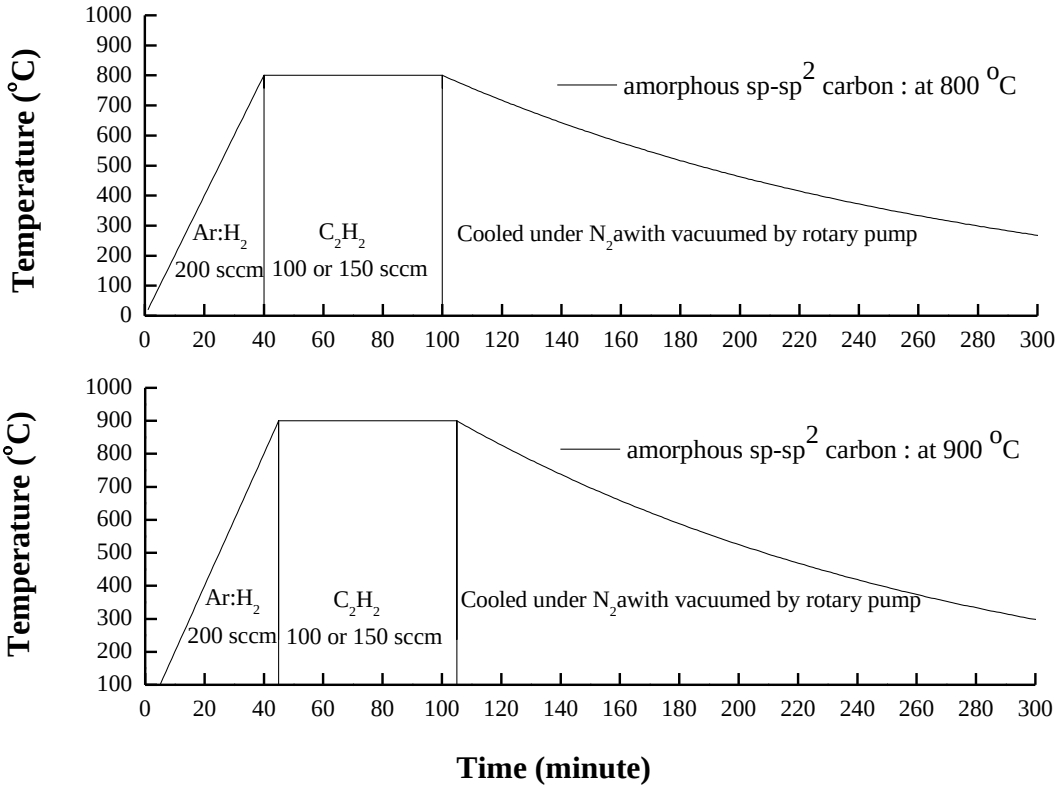

Figure 3.5 Flow of procedure to synthesis amorphous sp-sp^2 carbon films at (A) 800 °C and (B) 900 °C.

CHAPTER 4 RESULT AND DISCUSSION

4.1 Graphite films on texture SiO_2/Si wafers

Figure 4.1(A) shows texture of SiO_2/Si wafers. Figure 4.1(B) and (C) show the surface of the wafers after the deposition process. In this process, carbon was decomposed from hydrocarbon molecules (C_2H_2 gas) at temperatures of 800 °C and 900 °C. As seen on the Figure 4.1(A), (B) and (C), the different contrast has observed on the edge of surface due to the coated films was conformal and covered all substrate. The edge effect of uncoated specimen was mitigated due to the smoothening of the edge by the covered carbon.

Table 4.1 shows atomic percentage of Si, C and O on the texture SiO_2/Si wafers before and after deposition. The atomic percentages of all elements using mapping mode EDX spectroscopy at 500X. As expected, the atomic percentage of C increases and atomic percentage of Si decreases. This results confirm that the substrates in Figure 4.1(B, C) was covered by carbon. The low atomic percentage of O was a result of the formation of carbon on the surface of substrates and the escape depth of the X-ray was limited.

The sheet resistance of graphite films on the texture SiO_2/Si measured by 4-point probe measurement and shows in table 4.1. Graphite films deposited at 800 °C and 900 °C have sheet resistance of 221.44 and 84.52 Ω/sq, respectively. The decrease of sheet resistance was expected to be a result of the film thickness. It was expected that graphite films synthesis at 900 °C was possibly thicker than that of 800 °C due to the rate of deposition increase at higher growth temperature.

Figure 4.2 shows Raman spectra of graphite films as deposited on texture SiO_2/Si wafers. These spectra present three major important peaks, D (disorder) peak, G peak and 2D peak [19]. The Breit-Wigner-Fano line shape [20] was used to fit Raman spectrum in the range of 700-2200 cm^{-1} and the Gaussian function in the range of 2200 to 3000 cm^{-1}. The result of fitting: the peak position, the full width at half maximum (FWHM), the I_D/I_G ratio and the I_{2D}/I_G ratio, are summarized in table 4.2.

The Raman spectrum shows broad of D peak and narrow of G peak. While, the broadly of 2D peaks due to the overlap of many layer graphite planes. For graphite films grown at 800ºC, the center D peak, G peak and I_D/I_G are 1342 cm^{-1}, 1599 cm^{-1} and 0.71, respectively. And graphite films grown at 900 ºC, the centered D peak, G peak and I_D/I_G are 1350 cm^{-1}, 1596 cm^{-1} and 0.87, respectively.

The I_D/I_G was used to evaluate disordered graphite and in-plane crystalline (L_a). The L_a of graphite materials was calculated by Cancado equation (See eqution 2.3 section 2.6 in chapter 2):

$$L_a(nm) = (2.4 \times 10^{-10})\lambda_{laser}^4 \left(\frac{I_D}{I_G}\right)^{-1}$$

where λ is laser excitation wavelength in nm. From the calculation, L_a of graphite films growth at 800 °C and 900 °C are 24 nm and 19 nm, respectively. These films were classified into nano-crystalline graphite. The I_{2D}/I_G ratio of these films in the range of

~0.16-0.18 normally exists in bulk graphite materials. In graphene structure with less than five-layers, the I_{2D}/I_G ratio is about 2 to 4.

As increasing of growth temperature, G peak position moves slightly to lower wavenumber ($\Delta\omega$ = ~3 cm^{-1}). While, the FWHM of G peak and the I_D/I_G ratio increase, L_a decreases because the increase of disordered carbon.

Ferrari and Robertson [1, 21] described that G peak of graphite and glassy carbon does not disperse [E_{2g} symmetry at ~1581 cm^{-1}] but disperse in the case of disordered and amorphous carbon. The G peak in graphite cannot disperse because it is Raman-active phonon mode of the crystal.

Table 4.1 Atomic percentages of Si, C and O, and sheet resistance values of graphite films on SiO_2/Si substrates.

Samples	Atomic %			Sheet resistance (Ω/sq)
	Si	C	O	
Texture SiO_2/Si	76.74	2.83	19.97	NA
GF on SiO_2 (800 °C)	16.75	81.30	1.79	221.44
GF on SiO_2 (900 °C)	18.84	78.82	2.16	84.52

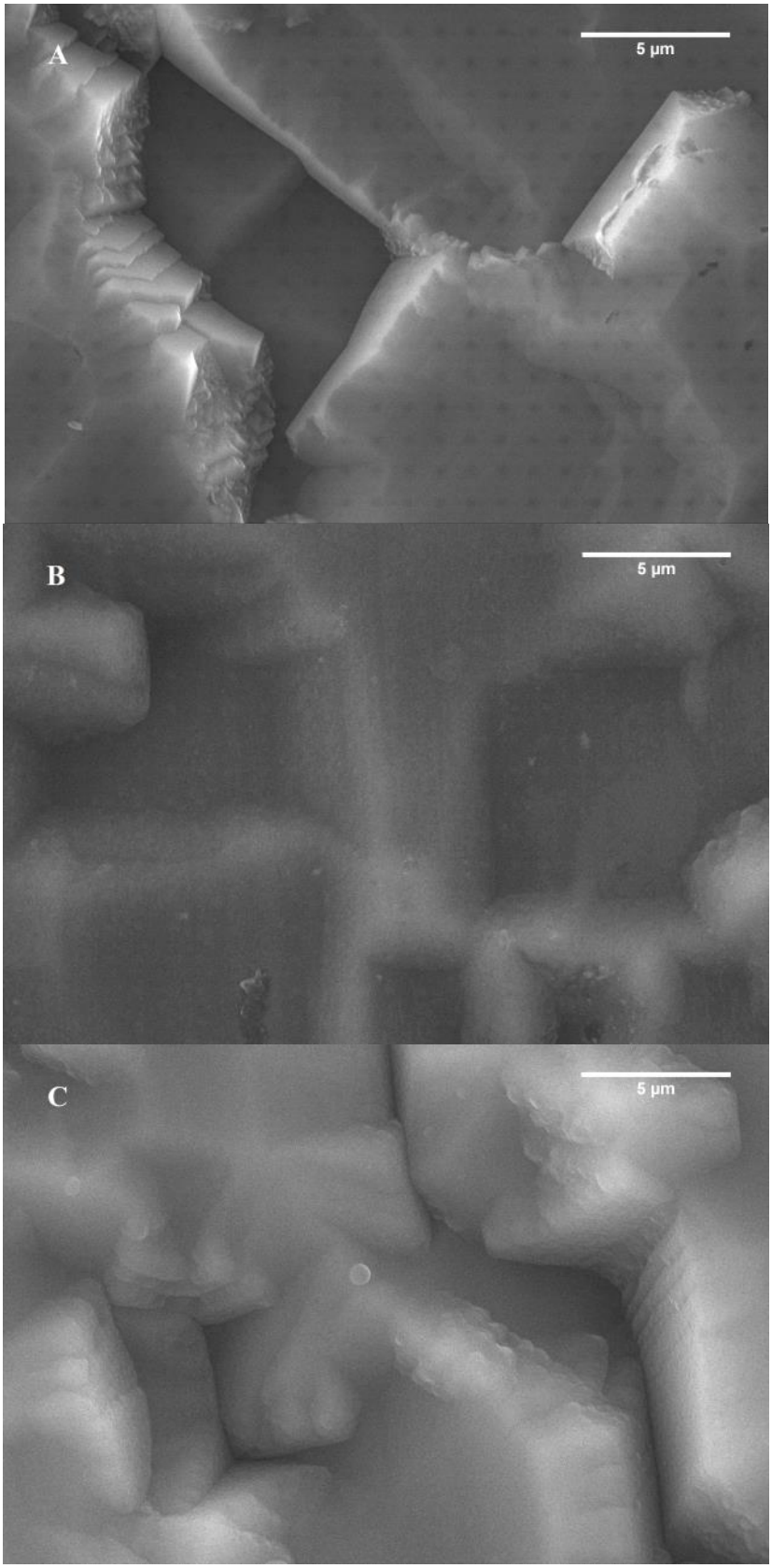

Figure 4.1 SEM images of (A) texture SiO_2/Si wafer, (B) and (C) are as deposited graphite films at 800 °C and 900 °C on texture SiO_2/Si wafer, respectively.

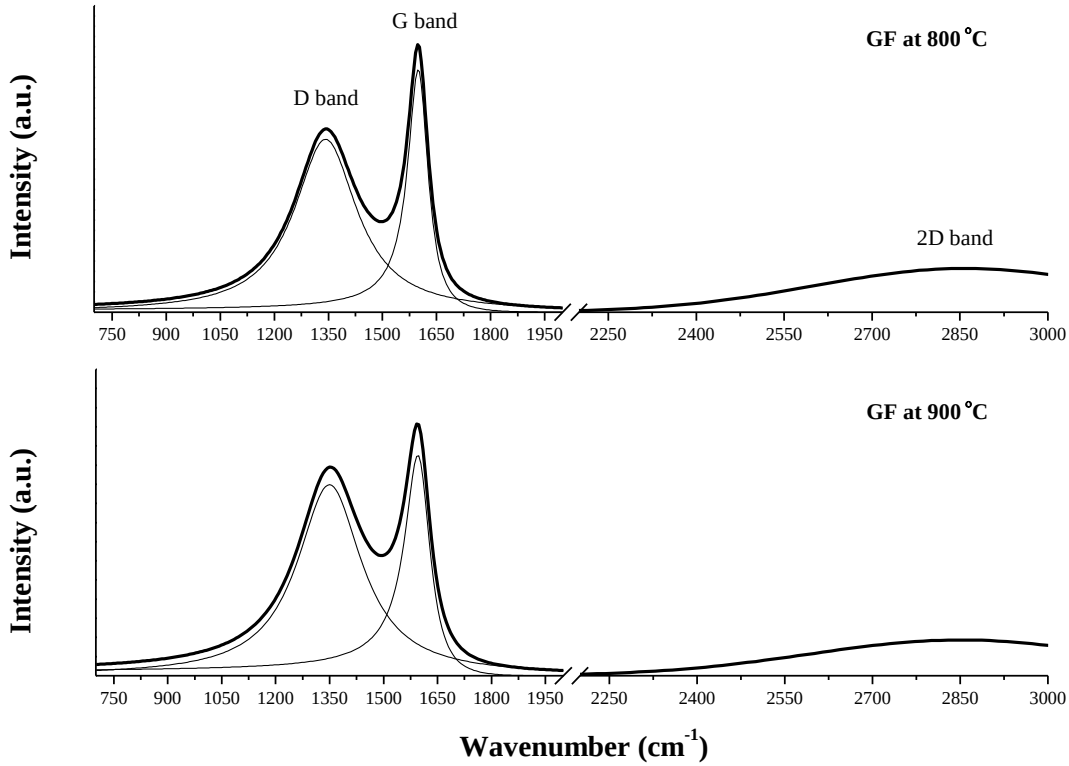

Figure 4.2 Raman spectra of GF synthesized at 800 °C and 900 °C fitted using Breit-Wigner-Fano (BWF) line shape.

Table 4.2 Peak positions and FWHM (denoted by Δ) of D, G and 2D band, I_D/I_G, I_{2D}/I_G, and estimate in-plane crystalline size (L_a) of graphite films.

Sample	D band		G band		2D band		I_D/I_G	I_{2D}/I_G	L_a (nm)
	Pos.	Δ	Pos.	Δ	Pos.	Δ			
GF-800	1342	211	1599	69	2860	606	0.71	0.18	24
GF-900	1350	218	1596	88	2851	610	0.87	0.16	19

4.2 Amorphous sp-sp^2 carbon on quartz slides

Figure 4.3 shows XRD patterns of amorphous sp-sp^2 carbon on quartz slides in the range of 20-80°. All of XRD spectra presence non-crystalline (002) peak center at ~21° [22]. The broadly of XRD spectra at low 2θ values of 13 to 24 degrees indicate the amorphous nature of material having some degree of arrangement (crystallinity) in the molecular chains [23]. The natural graphite has (002) peak position center at 26.54° [24]. The in-plane crystalline size (L_a) is calculated from the peak (002) by using the formula [22]

$$L_a = \frac{0.92\lambda}{\Delta sin\theta} \tag{4.1}$$

where λ is the wavelength of incident X-ray, Δ is the full width at a half maximum (FWHM), and θ is the diffraction angle. The 2θ, Δ, and La was summarize in table 4.4. The estimate crystalline size in a-axis (L_a) is ~18 Å.

Figure 4.4 shows the Infrared Raman spectra (laser Raman excitation at 758 nm) of as-deposited amorphous sp-sp^2 carbon films on quartz substrates. The overall Raman spectra in the range of 800-2200 cm^{-1} are look similarly in position and intensity when normalized data. The inset of Figure 4.4 is Raman spectrum of quartz substrate before deposited and shows ν_a(Si-O-Si) peak center at ~1083 cm^{-1} [25].

All of Raman spectra were smoothed by FFT (Fast Fourier transform) Filter and fitted by using Gaussian function. The result of fitting shows the superposition of D, G and C band (Figure 4.5 and data summarized in Table 4.4).

The D band existing in the Raman spectra presents the disordered peak and confirm that the films contain sp^2 ring. D peak is a breathing mode of A_{1g} symmetry in aromatic rings normally lie at ~1355 cm^{-1}. The G band is a stretching vibration of all pairs of sp^2 carbon in both rings and chains. The G band always lies in the range 1490-1630 cm^{-1} [1, 21]. The C band exiting in the range 1800-2200 cm^{-1} presents the monoatomic carbon linear chains. The C band could be divided to two different peak polyyne center at 1980 cm^{-1} and cumulene center at 2100 cm^{-1} (Raman laser excitation at 532 nm) [26-28].

The full width at half maximum (FWHM) of D peak is ~117 cm^{-1}, G peak varied in the range of ~531 ± 27 cm^{-1}, and C peak varied in the range ~235 ± 29 cm^{-1}. The center peak positions of D peak lie at ~1386 ± 5 cm^{-1}, G peak lie at ~1499 ± 1 cm^{-1}, and C peak lie at ~1903 ± 3 cm^{-1}.

The I_D/I_G ratio of this film is 0.56 which stay in second stage of three-stage model of Ferrari and Robertson [1] showing that this film has sp^3 C. However, to evaluate the sp^2 and sp^3 fraction by the I_D/I_G, nuclear magnetron resonance (NMR) or electron-energy-loss spectroscopy should be used complementary with Raman data.

The G peak position at ~1499 ± 1 cm^{-1} provcide the information of a formation of C=C chains in the polyacetylene-like structure (each sp^2 carbon atom bonded to hydrogen) [1, 29-32]. The G peak lie at ~1500 cm^{-1} mostly exits in hydrogenated amorphous carbon (a-C:H) at Raman excitation 633 nm, tetrahedral amorphous carbon at Raman excitation 633 nm, and tetrahedral hydrogenated amorphous carbon at Raman excitation

633 nm and 758 nm [21]. Wang et al. [32] synthesized a-C:H by Hot Filament PECVD from acetylene gas and reported that when the C_2H_2 flow exceed 40 sccm, the films tend to be more polymer-like structure because the dehydrogenation to produce such cross-liked network driven by energetic ions is believed to be hindered at higher C_2H_2 flow rate.

The C peak position of this films lie at ~1903 ± 3 cm^{-1} has lower wavenumber than the result of Casari et al. [28] and Ravagnan et al. [26,27] (roughly ~90 cm^{-1}) because the D, G and C peak normally shift to lower wavenumber at higher laser Raman excitation [1, 21]. Casari et al. [28] and Ravagnan et al. [26] reported the Raman spectra of amorphous sp-sp^2 carbon by varying laser excitation 532 and 632 nm, the C band under laser Raman excitation at 632 nm showed lower intensity and lower wavenumber than the C band at 532 nm.

As the increasing of growth temperature: the D, G and C peak dispersed slightly, the FWHM of G band has narrowed and C band has broadened while the D band and the I_D/I_G ratio does not significant change. The narrow G band reveals the sp^2 C fraction organized in aromatic rings increase and broadening of C band reveals the sp C containing on the films decreases. However, the effect of the increase of C_2H_2 flow rate on the structural of amorphous sp-sp^2 is still not clear in this evidence.

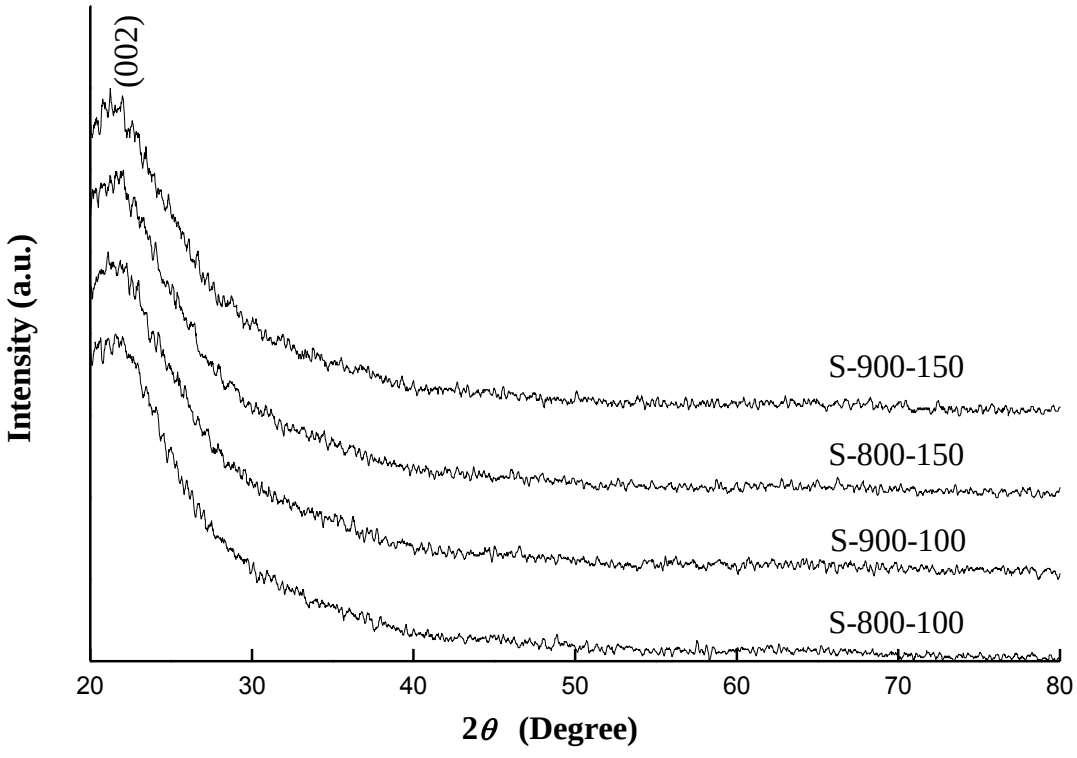

Figure 4.3 XRD patterns of amorphous sp-sp^2 carbon grown with different temperature and acetylene flow rate (Specimen-Temp-Flow Rate).

Table 4.3 2θ, FWHM (denoted by Δ), and L_a from the XRD spectra.

S-Temp-Flow	2θ	Δ	L_a (Å)
S-800-100	21	22	20
S-900-100	20	26	18
S-800-150	21	25	18
S-900-150	21	25	18

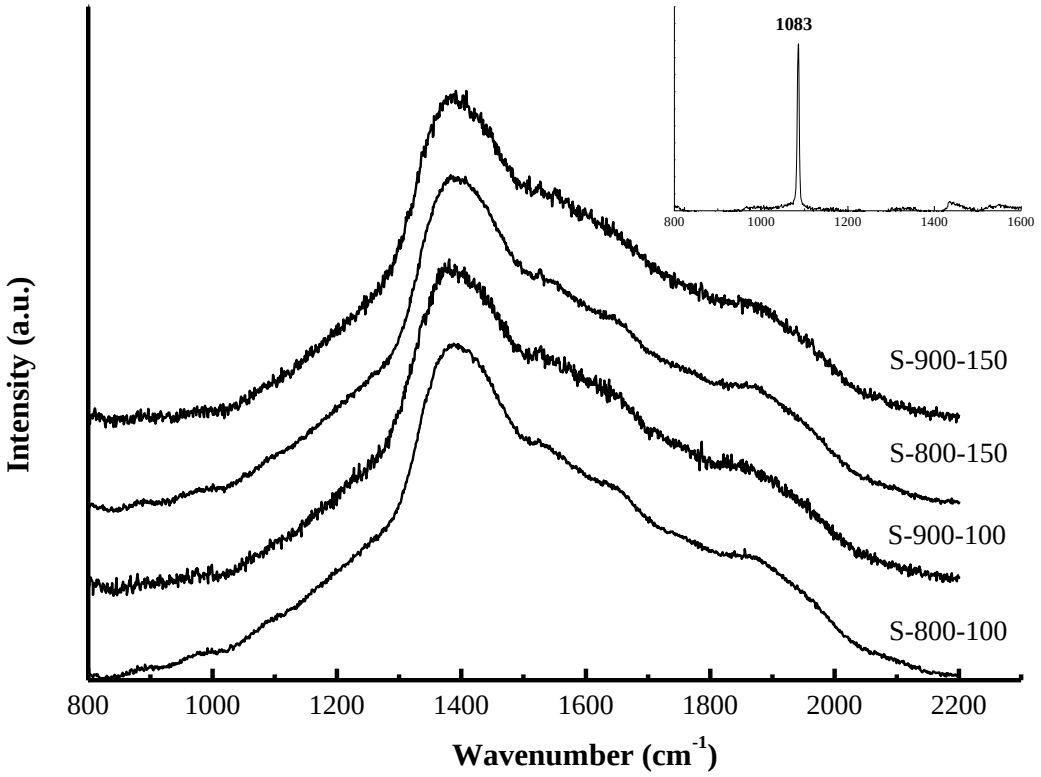

Figure 4.4 Raman spectrum of a-C with sp hybridization prepared by Thermal-CVD from (Specimen-Temp-Flow). The inset of figure is Raman spectrum of quartz slides before deposited.

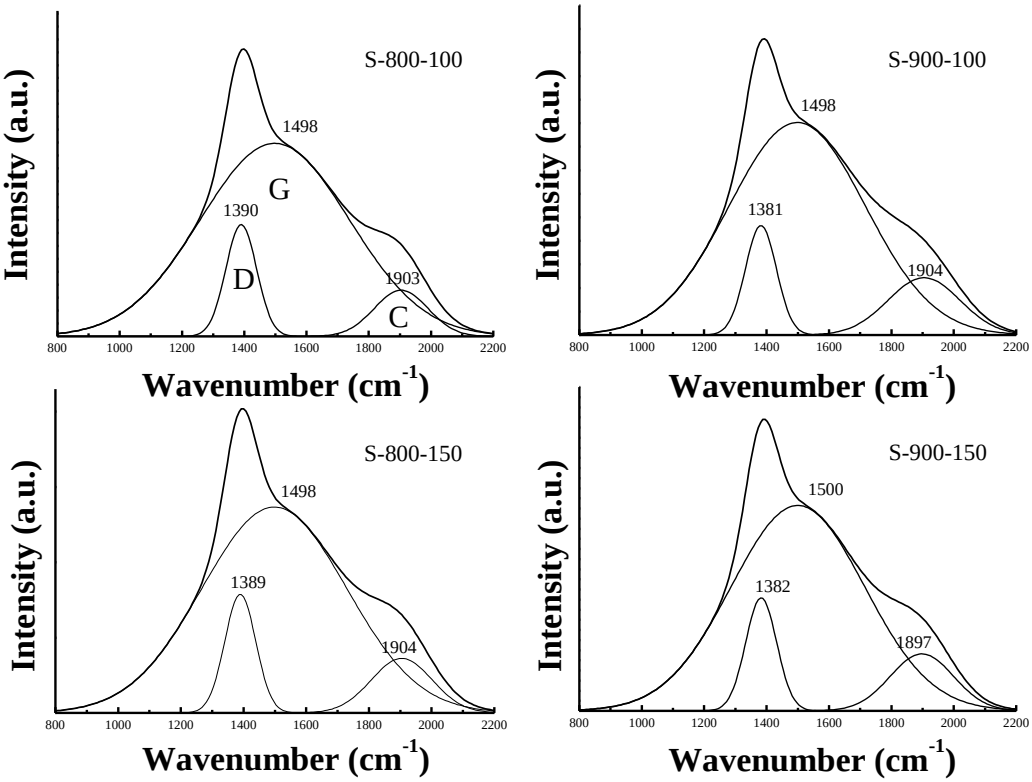

Figure 4.5 Individual deconvolve fitting of the Raman spectra in Figure 4.4.

Table 4.4 The peak positions and FWHM of D, G, and C band, and the I_D/I_G ratio from the Raman spectrum.

S-Temp-Flow	D-band		G-band		C-band		I_D/I_G
	Pos.	Δ	Pos.	Δ	Pos.	Δ	
S-800-100	1390	116	1498	563	1903.9	203.2	0.58
S-900-100	1382	117	1498	515	1904.6	272.3	0.52
S-800-150	1390	116	1498	543	1905.0	228.2	0.58
S-900-150	1383	117	1500	503	1897.9	239.2	0.55

Figure 4.6 and 4.7 show surface morphology of amorphous sp-sp^2 carbon films on quartz slides observed by SEM at magnification 2000X. All of specimens show graphite flake dispersed on the matrix of amorphous carbon. The micro-crack clearly seen on the films grown with C_2H_2 flow rate 100 sccm (Figure 4.7A and B) but not seen on the films grown with C_2H_2 flow rate 150 sccm. It is suggested that at the higher C_2H_2 flow rate may have higher intrinsic stress [33,34]. The intrinsic stress occurred by the different in thermal expansion coefficient of the substrate, and the growing carbon films.

Table 4.5 shows atomic percentages of C, Si and O, transmittance (%T), and sheet resistance after deposition. As expected, the atomic percentage of C has increase, transmittance values has decrease, and sheet resistance decreases when deposited at higher temperature because the films are thicker. The thickness of our films were approximate by the calculation from the transmittance (%T) spectra in Figure 4.8.

Figure 4.9 shows the relationship between sheet resistance and transmittance at 550 nm. For comparison, the theoretical sheet resistance of graphene layer, few layer graphene on glass slides [5], thin graphite films on sapphire [6] and amorphous sp-sp^2 carbon films on quartz slides were plotted. The amorphous sp-sp^2 carbon films had higher sheet resistance than that of FLG on glass slides but close to that of GF on sapphire substrate. The theoretical sheet resistance (R) was calculated using the following equation as a function of transmittance (T):

$$R = \frac{-4\pi k}{G\lambda lnT} \tag{4.2}$$

where k is the excitation coefficient ($k = 1.3$), G is the conductivity ($G = 2.1 \times 10^6$), and λ is the wavelength of incident light [35].

The sheet resistance of this film is higher than theoretical and experiment of graphene but equivalent with thin graphite films. Cai et al. [5] reported that the sheet resistance of few layer graphene was higher than the theoretical graphene layer because small cracks were formed during the transfer process and the films had some defect on the structure due to the observed small D peak on the Raman spectra. However, in their Raman spectra had the I_D/I_G ~0.05 order which suggested that the films had few defect and had good in crystal quality. On the other hand, the sheet resistance of thin graphite films and amorphous sp-sp^2 carbon is higher by ~2 orders of magnitude than that of theoretical value. The thin graphite films synthesized by Miyasaka et al. had higher sheet resistance because of the films consisted of nanograins (~8.7-14.3 nm) and the presence of the defect because the D peak observed with high of the I_D/I_G ratio (~1.33-2.19 order). While, amorphous sp-sp^2 carbon has higher sheet resistance because the XRD and Raman spectra presents the amorphous structure and the micro-crack observed on the films. However, the effect of monoatomic carbon linear chains or sp C [36] also enhanced the sheet resistance of amorphous carbon to be equivalent with thin graphite films from the reported of Miyasaka et al.

Table 4.5 The atomic percentages of C, Si and O, transmittance (%T), and sheet resistance values of amorphous sp-sp^2 carbon films.

S-Temp-Flow	Atomic %			Transmittance (%T)	Sheet resistance (kΩ/sq.)
	C	Si	O		
S-800-100	3	31	66	82	9.1
S-900-100	14	26	59	31	0.6
S-800-150	3	31	66	78	8.9
S-900-150	11	27	62	31	1.2

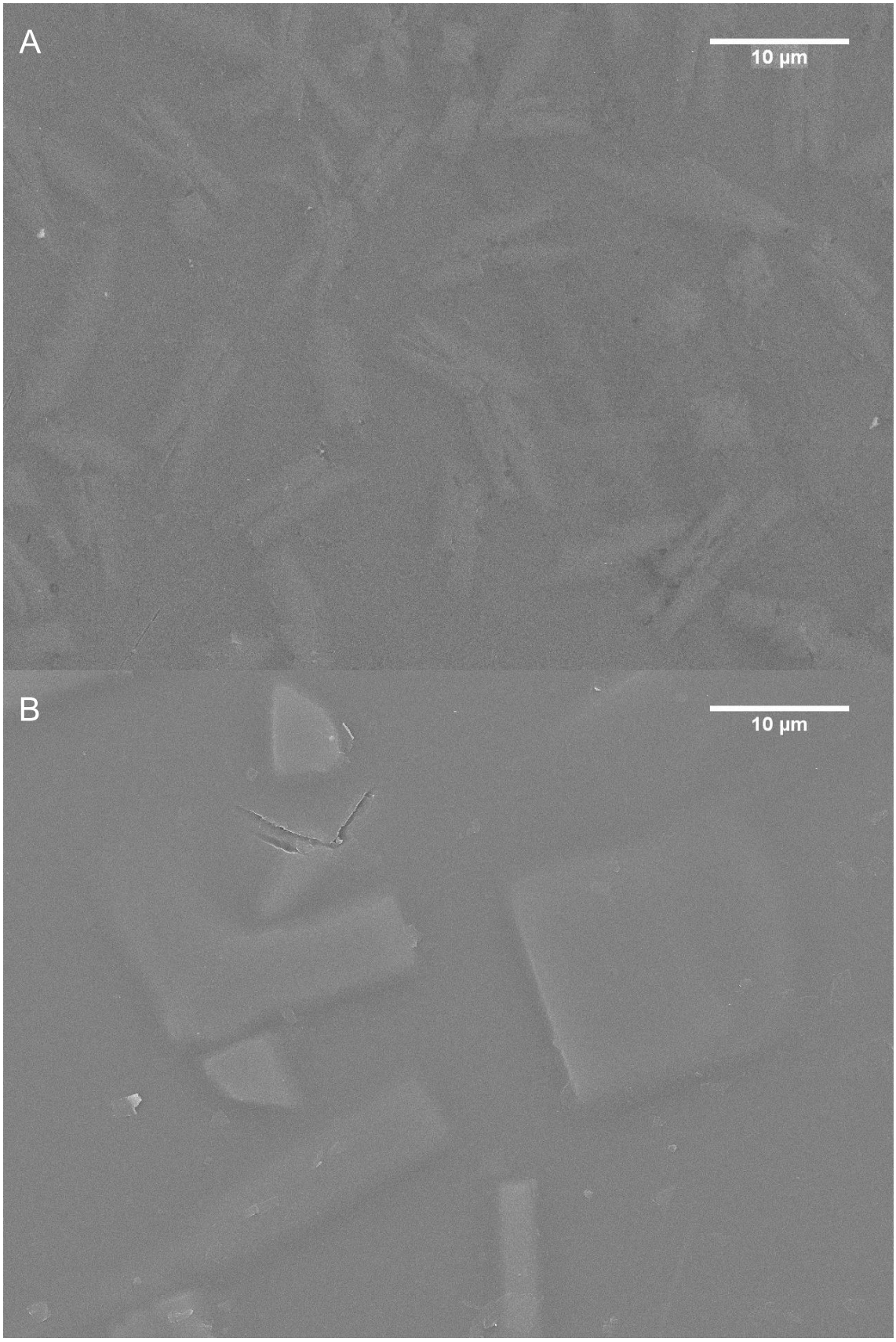

Figure 4.6 Surface morphology of amorphous sp-sp^2 growth at (A) 800 °C and (B) 900 °C with C_2H_2 flow rate 100 sccm.

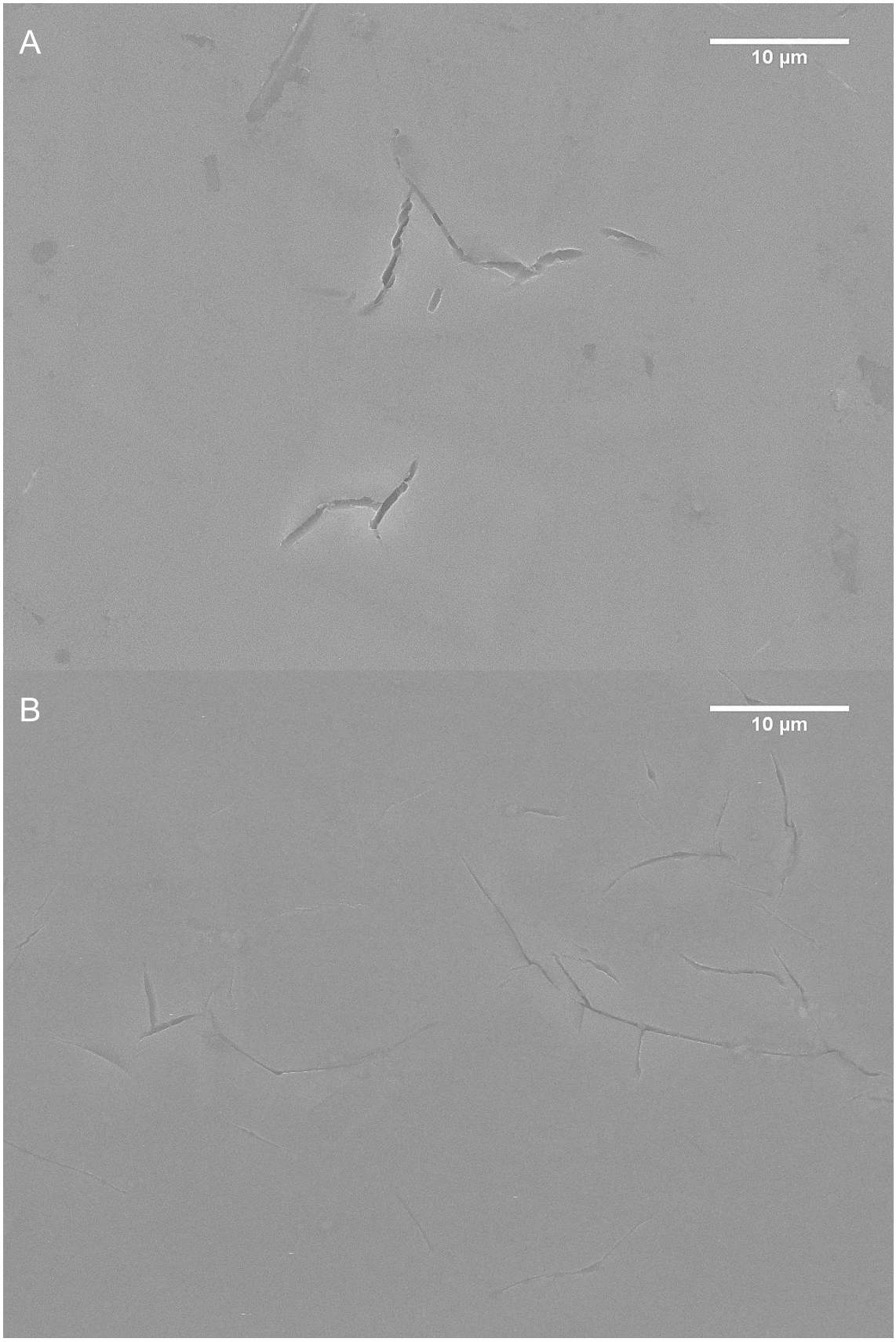

Figure 4.7 Surface morphology of amorphous sp-sp^2 carbon growth at (A) 800 °C and (B) 900 °C with C_2H_2 flow rate 150 sccm.

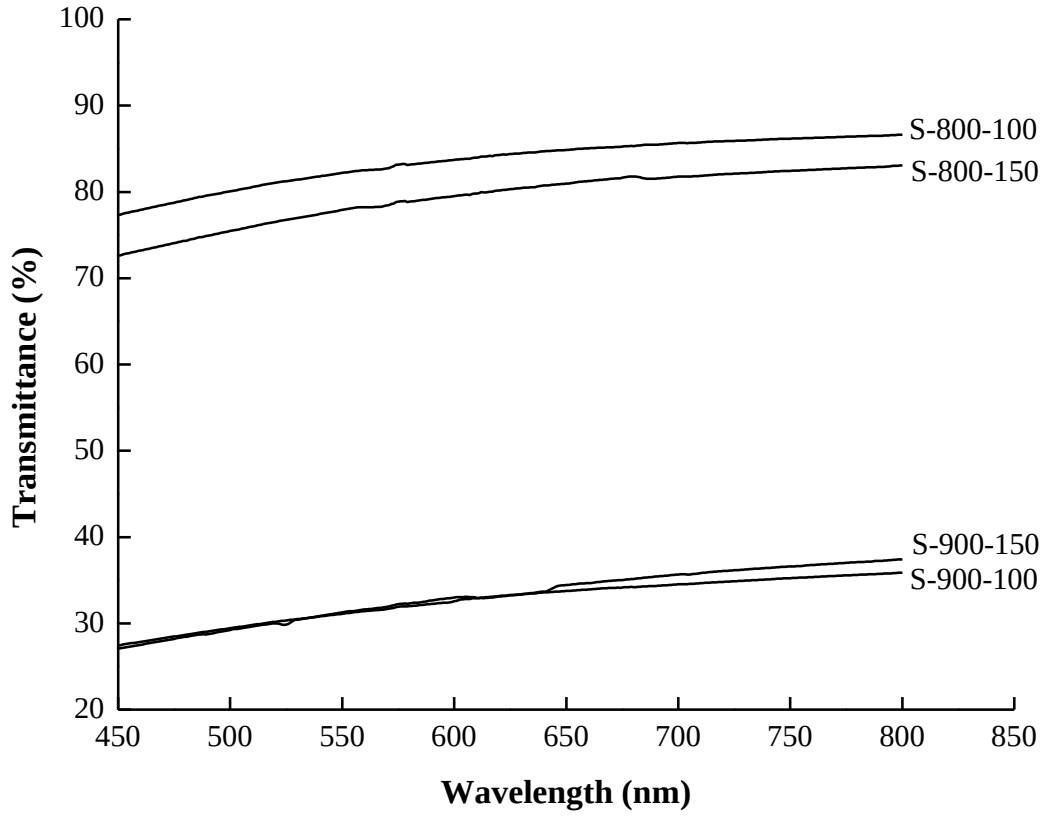

Figure 4.8 Transmittance spectrum of amorphous sp-sp^2 carbon (Specimen-Temp-Flow).

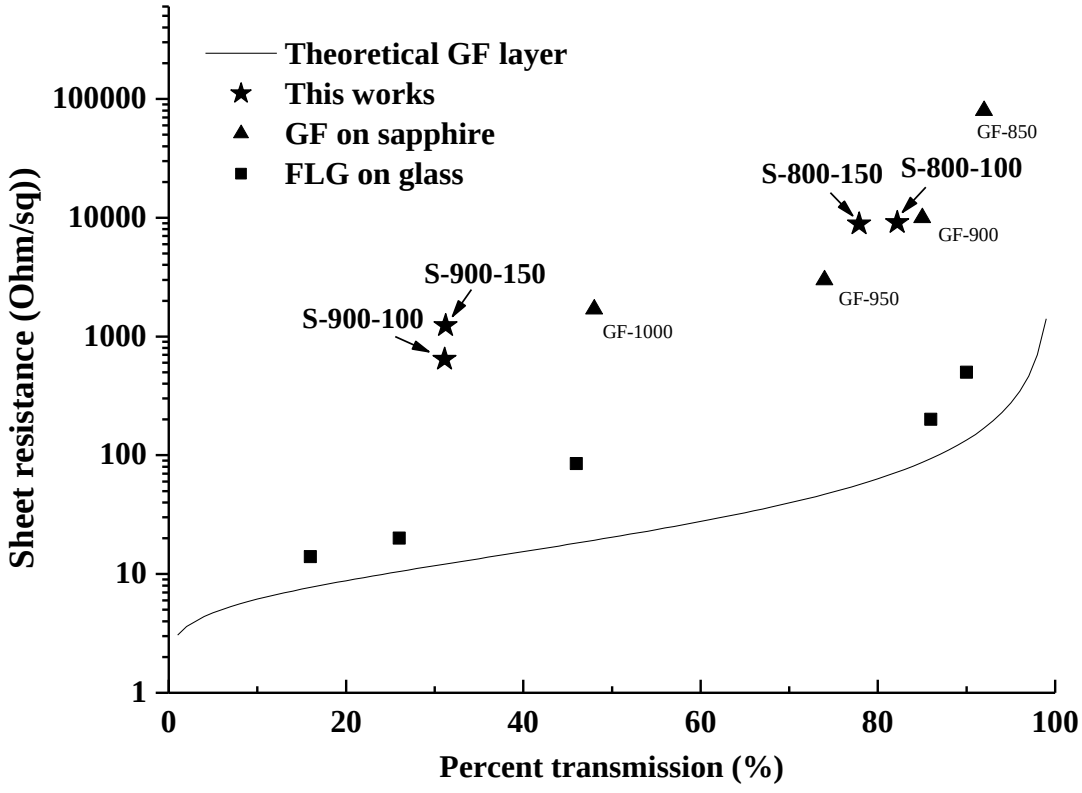

Figure 4.9 Plot of sheet resistance as a function of transmittance at 550 nm.

CHAPTER 5 CONCLUSION AND SUGGESTION

On the first experiment, carbon films were grown on texture SiO_2/Si wafers without metal seed layer by TCVD at 800 °C and 900 °C with C_2H_2 flow rate 40 sccm under atmospheric pressure. Raman spectrum shows graphite structure with the I_D/I_G of ~0.7-0.9 with the estimated in-plane crystalline size of ~19-24 nm. As the growth temperature increased to 900 °C, the Raman spectra showed that the I_D/I_G ratio and the FWHM of G peak increased due to the increase of disordered of sp^2 carbon. The decomposition of C_2H_2 gas at the temperature in the range 800-900 °C could deposit graphite films or many layer graphene on the transparent substrate such as quartz slides without metal seed layer.

In the second experiment, carbon films were grown on quartz slides without metal seed layer at 800 and 900 °C with C_2H_2 flow rate 100 and 150 sccm under pressure of 15 mbar. The Raman spectrum presented the amorphous sp^2 carbon coexisted with sp carbon (C band). The sp carbon are not commonly to observe in Raman spectrum on the amorphous sp^2 carbon. The sp carbon (Polyyne and Cumulene) was predicted by theoretical that has extremely on the electronic structure. The sp carbon containing in this film possibly enhanced the conductivity of amorphous carbon which is equivalent with thin graphite films. As increasing growth temperature to 900 °C, the Raman spectra presents that the FWHM of G peak decreased and the FWHM of C peak increased. This showed that the sp^2 carbon fraction contained in this films increased and sp carbon decreased. However, it is believe that the sheet resistance of this films could be reduce by improve the crystalline structure of sp^2 carbon and sp carbon by optimize experiment conditions either treat substrate surfaces or annealing carbon films in high vacuum.

REFERENCE

1. Ferrari, A.C. and Robertson, J., 2000, "Interpretation of Raman Spectra of Disordered and Amorphous Carbon", **Physical Review B**, Vol. 61, No. 20, pp. 14095-14107.

2. Reina, A., Jia, X., Ho, J., Nezich, D., Son, H., Bulovic, V., Dresselhaus, M.S. and Kong, J., 2009, "Large Area, Few Layer Graphene Films on Arbitrary Substrates by Chemical Vapor Deposition", **Nano Letters**, Vol. 9, No. 1, pp. 30-35.

3. Li, X., Zhu, Y., Cai, W., Borysiak, M., Han, B., Chen, D., Piner, R.D., Colombo, L. and Ruoff, R.D., 2009, "Transfer of Large-Area Graphene Films for High-Performance Transparent Conductive Electrodes", **Nano Letters**, Vol. 9, No. 12, pp. 4359-4363.

4. Kim, K.S., Zhao, Y., Jang, H., Lee, S.Y., Kim, J.M., Kim, K.S. Ahn, J.H., Kim, P., Choi, J.Y. and Hong, B.H., 2009, "Large-Scale Pattern Growth of Graphene Films for Strechable Transparent Electrodes", **Nature Letters**, Vol. 457, pp. 706-710.

5. Cai, W., Zhu, Y., Li, X., Piner, R.D. and Ruoff, R.D., 2009, "Large Area Few-Layer Graphene/Graphite Films as Transparent Thin Conducting Electrodes", **Applied Physics Letters**, Vol. 95, p. 123115.

6. Miyasaka, Y., Nakamura, A. and Temmyo, J., 2011, "Graphite Thin Films Consisting of Nanograins of Multilayer Graphene on Sapphire Substrates Directly Grown by Alcohol Chemical Vapor Deposition", **Japanese Journal of Applied Physics**, Vol. 50, p. 04DH12.

7. Nakamura, A., Miyasaka, Y. and Temmyo, J., 2012, "Direct Growth Properties of Graphene Layers on Sapphire Substrate by Alcohol-Chemical Vapor Deposition", **Japanese Journal of Applied Physics**, Vol. 51, p. 04DN03.

8. Spain, I.L., 1981, "Electronic Transport Properties of Graphite, Carbons, and Related Materials", **Chemistry and Physics of Carbon**, Vol. 16, pp. 126-127.

9. Dresshaus, M.S., Dresshaus, G. and Eklund, P.C., 1996, **Science of Fullerenes and Carbon Nanotubes**, Academic Press, San Diego, pp. 17-18.

10. Bundy, F.P., Bassett, W.A., Weathers, M.S., Hemley, R.J., Mao, H.K. and Goncharov, A.F., 1996, "The Pressure-Temperature Phase and Transformation Diagram for Carbon; Updated Through 1994", **Carbon**, Vol. 3, No. 2, pp. 141-153.

11. Robertson, J., 2002, "Diamond-Like Amorphous Carbon", **Materials Science and Engineering**, Vol. 37, pp. 129-131.

12. Wallace, P.R., 1946, "The Band Theory of Graphite", **Physical Review**, Vol. 71, No. 9, pp. 622-634.

13. Fuhrer, M.S., Lau, C.H., and MacDonald, A.H., 2010, "Graphene: Materially Better Carbon", **Materials Research Society**, Vol. 35, pp. 289-295.

14. Jacob, W. and Möller, W., 1993, "On The Structure of Thin Hydrocarbon Films", **Applied Physics Letters**, Vol. 63, pp. 1771-1773.

15. Jorio, A., Dresselhaus, M., Saito, R. and Dresselhaus, G.F., 2011, **Raman Spectroscopy in Graphene Related Systems**, WILEY-VCH, Weinheim, pp. 73-101.

16. Long, D.A., 1977, **Raman Spectroscopy**, McGraw-Hill, Maidenhead, pp. 1-13.

17. Cancado, L.G., Takai, K. and Enoki, T., 2006, "General Equation for The Determination of the Crystalline Size L_a of Nanographite by Raman Spectroscopy", **Applied Physics Letters**, Vol. 88, p. 163106.

18. Ferrari, A.C., Meyer J.C., Scardaci, V., Casiraghi, C., Lazzeri, M., Mauri, F., Piscanec, S. and Jiang, D., 2006, "Raman Spectrum of Graphene and Graphene Layers", **Physical Review Letter**, Vol. 97, p. 187401.

19. Ferrari, A.C., 2007, "Raman Spectroscopy of Graphene and Graphite : Disorder, Electron-Phonon Coupling, Doping and Nonadiabatic Effects", **Solid State Communications**, Vol. 143, pp. 47-57.

20. Prawer, S., Nugent, K.W., Lifshitz, Y., Lempert, G.D., Grossman, E., Kulik, J., Avigal, I. and Kalish, R., 1996, "Systematic Variation of The Raman Spectra of DLC Films as a Function of sp^2:sp^3 composition", **Diamond and Related Materials**, Vol. 5, pp. 433-438.

21. Ferrari, A.C. and Robertson, J., 2001, "Resonant Raman Spectroscopy of Disordered, Amorphous, and Diamondlike Carbon", **Physical Review B**, Vol. 24, p. 75414.

22. Zhao, J., Yang, L., Li, F., Yu, R. and Jin, C., 2009, "Structural Evolution in The Graphitization Process of Activated Carbon by High-Pressure Sintering", **Carbon**, Vol. 47, pp. 744-751.

23. Cullity, B.D. and Stock, S.R., 2001, **Elements of X-Ray Diffraction**, 3rd ed., Prentice Hall, New Jersey, pp. 182-183.

24. Sun, G., Li. X., Qu, Y., Wang, X., Yan, H. and Zhang, Y., "Preparation and Characterization of Graphite Nanosheets from Detonation Technique", **Materials Letters**, Vol. 62, pp. 703-706.

25. Long, D.A., 1977, **Raman Spectroscopy**, McGraw-Hill, Maidenhead, p. 158.

26. Ravagnan, L., Siviero, F., Lenardi, C., Piseri, P., Barborini, E., Milani, P., Casiri, C.S., Bassi, A.L. and Bottani, C.E., 2002, "Cluster-Beam Deposition and In Situ Characterization of Carbyne-Rich Carbon Films", **Physical Review Letters**, Vol. 89, p. 285506.

27. Ravagnan, L., Piseri, P., Bruzzi, M., Bongiorno, G., Baserga, A., Casari, C.S., Bassi, A.Li., Lenardi, C., Yamaguchi, Y., Wakabayashi, T., Bottani, B.E. and Milani, P., 2007,

"Influence of Cumulene Chains on the Vibrational and Electronic Properties of sp/sp^2 Amorphous Carbon", **Physical Review Letters**, Vol. 98, p. 216103.

28. Casari, C.S., Bassi, A.L., Baserga, A., Ravagnan, L., Piseri, P., Lenardi, C., Tommasini, M., Milani, A., Fazzi, D., Bottani, C.E. and Milani, P., 2008, "Low Frequency Modes in the Raman Spectrum of sp^2-sp^3 Nanostructured Carbon", **Physical Review B**, Vol. 77, p. 195444.

29. Piazza, F., Golanski, A., Schulze, S. and Relihan, G., 2003, "Transpolyacetylene Chains in Hydrogenated Amorphous Carbon Films Free of Nanocrystalline Diamond", **Applied Physics Letters**, Vol. 82, pp. 358-360.

30. May, P.W., Smith, J.A. and Rosser, K.N., 2008, "785 nm Raman Spectroscopy of CVD Diamond Films", **Diamond and Related Materials**, Vol. 17, pp. 199-203.

31. Silinskas, M., Grigonis, A., Kulikauskas, V. and Manika, I., 2008, "Hydrogen Influence on the Structure and Properties of Amorphous Hydrogenated Carbon Films Deposited by Direct Ion Beam", **Thin Solid Films**, Vol. 516, pp. 1683-1692.

32. Wang, J., Zhang, S., Wang, H., Wong, K., Zhou, Q. and Zhou, Y., 2009, "Kinetics and Characterization of Hydrogenated Carbon with Ruthenium Interlayer", **Thin Solid Films**, Vol. 517, pp. 5202-5206.

33. Abbas, G.A., Roy, S.S., Papakonstantinou, P. and McLaughlin, J.A., 2005, "Structural Investigation and Gas Barrier Performance of Diamond-like Carbon Based Films on Polymer Substrates", **Carbon**, Vol. 43, pp. 303-309.

34. Abbas, G.A., McLaughlin, J.A. and Harkin-Jones, E., 2004, "A Study of ta-C, a-C:H and Si-a:C:H Thin Films on Polymer Substrates as a Gas Barrier", **Diamond and Related Materials**, Vol. 13, pp. 1342-1345.

35. Soule, D.E., 1958, "Magnetic Field Dependence of the Hall Effect and Magnetoresistance in Graphite Single Crystals", **Physical Review**, Vol. 112, pp. 698-707.

36. Zhang, Y.Z., Su, Y., Wang, L., Kong, E.S., Chen, X. and Zhang, Y., 2011, "A One Dimensional Extremely Covalent Material: Monatomic Carbon Linear Chain", **Nanoscale Research Letter**, Vol. 6, p. 577.

CURRICULUM VITAE

NAME Mr. Somboon Fongchaiya

DATE OF BIRTH 30 December 1988

EDUCATIONAL RECORD

HIGH SCHOOL	High School Graduation Surawittayakarn School, 2007
BACHELOR'S DEGREE	Bachelor of Science (Physics) King Mongkut's University of Technology Thonburi, 2011
MASTER'S DEGREE	Master of Science (Physics) King Mongkut's University of Technology Thonburi, 2014

SCHOLARSHIP Research Assistant Scholarship
Thailand Center of Excellent in Physics

PUBLICATION

NATIONAL CONFERENCE

1. Fongchaiya, S., Jutarosaga, T., Denchitcharoen, S., Panichakarn, H., and Panthong, W., 2011, "The Investigation of Crown, Camber and Twist of Slider Bar with Laser Diode attachment and Relief Cut", **The 6th Annual Conference of The Thai Physics Society, Siam Physics Congress (SPC 2011)**, 23-26 March 2011, Ambassador City Jomtien Hotel, Pattaya, Thailand, pp. 248.

2. Fongchaiya, S., Tuayjaroen, R., Hassadee, A., Onreabroy, W., and Jutarosaga, T., 2012, "Seed Mediated Templateless Electrodeposition of Ag Nanostructure", **The 7th Annual Conference of The Thai Physics Society, Siam Physics Congress (SPC 2012)**, 9-12 May 2012, Phra Nakhon Si Ayutthaya, Thailand, pp. 254.

3. Fongchaiya, S., and Jutarosaga, T., 2013, "Effect of Growth Temperature on The Synthesis of Graphite Films on The Textured Si and SiO2/Si Wafers by Thermal Chemical Vapor Deposition Technique", **The 39th Congress on Science and Technology of Thailand (STT 39), 21-23 October 2013**, Bangkok International Trade & Exhibition Centre (BITEC) Bangkok, Thailand, pp. 470-476.